Journal of Fluid Mechanics

Evidence of very long meandering features in the logarithmic region of turbulent boundary layers

N. HUTCHINS and IVAN MARUSIC

Evidence of very long meandering features in the logarithmic region of turbulent boundary layers

N. HUTCHINS AND IVAN MARUSIC

Walter Bassett Aerodynamics Laboratory, Mechanical and Manufacturing Engineering, University of Melbourne, Victoria 3010, Australia

A regime of very long meandering positive and negative streamwise velocity fluctuations, that we term 'superstructures', are found to exist in the log and lower wake regions of turbulent boundary layers. Measurements are made with a spanwise rake of 10 hot-wires in two separate facilities (spanning more than a decade of Re_τ) and are compared with existing PIV and DNS results. In all cases, we note evidence of a large-scale stripiness in the streamwise velocity fluctuations. The length of these regions can commonly exceed 20δ. Similar length scales have been previously reported for pipes and DNS channel flows. It is suggested that the true length of these features is masked from single-point statistics (such as autocorrelations and spectra) by a spanwise meandering tendency. Support for this conjecture is offered through the study of a synthetic flow composed only of sinusoidally meandering elongated low- and high-speed regions. From detailed maps of one-dimensional spectra, it is found that the contribution to the streamwise turbulence intensities associated with the superstructures appears to be increasingly significant with Reynolds number, and scales with outer length variables (δ). Importantly, the superstructure maintains a presence or footprint in the near-wall region, seeming to modulate or influence the near-wall cycle. This input of low-wavenumber outer-scaled energy into the near-wall region is consistent with the rise in near-wall streamwise intensities, when scaled with inner variables, that has been noted to occur with increasing Reynolds number. In an attempt to investigate these structures at very high Reynolds numbers, we also report on recent large-scale sonic anemometer rake measurements, made in the neutrally stable atmospheric surface layer. Preliminary results indicate that the superstructure is present in the log region of this atmospheric flow at $Re_\tau = 6.6 \times 10^5$, and has a size consistent with outer scaling.

1. Introduction

Prior to the advent of particle image velocimetry (PIV) and direct numerical simulation (DNS) data, the precise form of the dominant log-region structure was largely unclear, although statistics based on fluctuating streamwise velocity (u) signals at these heights (particularly the peak in the premultiplied energy spectra $k_x \Phi_{uu}$ and the long tails in the autocorrelations) had long hinted at the existence of highly elongated regions of uniform streamwise momentum. Elegant, yet laborious, spatio-temporal two-point correlations (performed using a static and traversing hot-wire probe) revealed the time-averaged scale and form of these structures (Kovasznay, Kibens & Blackwelder 1970; Nakagawa & Nezu 1981; McLean 1990; Wark, Naguib & Robinson 1991). However, the first instantaneous snapshots of these structures were provided experimentally by PIV. Measurements in the streamwise/spanwise plane reveal that

the log region appears to be characterized by its own streaky structure, notably at a much larger scale than the well-documented near-wall streaks (Kline *et al.* 1967). Tomkins & Adrian (2003) and Ganapathisubramani *et al.* (2003) show instantaneous PIV examples of the u stripiness in the log region. Long regions of streamwise momentum deficit are found, with high-speed fluid seeming to fill the separation between neighbouring motions. Further investigations have suggested that these long modes of uniform momentum deficit are associated with packets of hairpin vortices (Adrian, Meinhart & Tomkins 2000; Tomkins & Adrian 2003; Ganapathisubramani, Longmire & Marusic 2003). It was found that the elongated low-speed regions are flanked by vortical motions (believed to be the necks of hairpin structures) and that together these features are dominant contributors to the overall Reynolds shear stress at this height (Ganapathisubramani *et al.* 2003; Marusic & Hutchins 2006). The low-speed regions are of the order 0.3–0.5δ wide, and typically have a length that exceeds the streamwise extent of the PIV frame (usually limited to $\sim 2\delta$). Instantaneous examples of these features are given in §3 (figure 1). Here δ is the boundary layer thickness, and the axis system x, y and z refer to the streamwise, spanwise and wall-normal directions, with u, v and w describing the respective fluctuating velocity components.

There is some evidence in the literature that these features can attain very large streamwise dimensions in pipes, channel flows and atmospheric surface layers. From hot-film measurements in pipe flows, Kim & Adrian (1999) and Guala, Hommema & Adrian (2006) found that streamwise energetic modes can extend up to 12–14 pipe radii, and refer to these as *very large-scale motions* (VLSM). Kim & Adrian (1999) suggest that the VLSM may be agglomerations of hairpin packets (themselves agglomerations of individual hairpin vortices). More recent analysis of large numerical domain DNS results (in particular two-dimensional spectra) have shown that in the log region, Φ_{uu} energy can reside in very long streamwise modes for larger k_y bands (certainly $>20h$, where h is the channel half-height – see del Álamo & Jiménez 2003; Jiménez 1998). Jiménez & del Álamo (2004) attribute the very long u fluctuations in the log region to 'passive wakes' formed downstream of smaller attached clusters of vortices. Similar models were suggested by Kovasznay and coworkers (Kovasznay 1970; Kovasznay *et al.* 1970; Blackwelder & Kovasznay 1972). Large streak-like features have also been noted in the atmospheric surface layer, both in experiments and LES studies (Drobinski *et al.* 2004; Young *et al.* 2002) and have been referred to by Phillips (2003) as *atmospheric Langmuir circulations* (ALC), implying a formation mechanism similar to roll-cells observed in the oceans and other bodies of water.

In light of these suggested length scales, and in recognition of the limited fields of view afforded by PIV, we here employ a spanwise rake of 10 hot-wire sensors in an attempt to capture the true extent of the largest scales. The idea is to use the fluctuating signals from the rake to reconstruct the instantaneous spanwise profile of the u velocity fluctuation. By projecting this signal in time and using Taylor's hypothesis (frozen convection) a view of the long high- and low-speed streaks can be constructed that covers a much larger streamwise domain than that attainable from PIV.

2. Experimental set-up

The hot-wire rake consists of 10 Dantec 55P16 single sensor hot-wire probes with a spanwise spacing (s_y) of approximately 0.115δ, such that the entire rake measures a spanwise domain just greater than one boundary layer thickness. The probes have 1.25 mm long platinum-plated tungsten wire sensing elements of 5 μm diameter and are operated in constant temperature mode using an AA Lab Systems AN-1003

Re_τ	Facility	δ (m)	U_τ (m s^{-1})	U_∞ (m s^{-1})	l^+	s_y/δ		T^+	z/δ 0.05	0.10	0.15	0.50
1120	Minnesota	0.069	0.24	6.0	17	0.114		0.4	—	—	✓	✓
7610	Melbourne	0.336	0.34	9.82	23	0.118	(0.030)	0.8	✓	✓	✓	✓
14 380	Melbourne	0.328	0.67	20.4	45	0.122	(0.030)	3.0	✓	✓	✓	✓
19 960	Melbourne	0.321	0.96	29.8	63	0.125	(0.031)	6.1	✓	✓	✓	✓

TABLE 1. Experimental parameters for hot-wire rake experiments.

Re_τ	Facility	δ (m)	U_τ (m s^{-1})	U_∞ (m s^{-1})	l^+	T^+
1010	Minnesota	0.070	0.22	5.2	14	0.1
1910	Minnesota	0.064	0.47	12.1	30	0.7
2630	Minnesota	0.066	0.62	16.9	40	0.6
4110	Minnesota	0.061	1.06	29.6	67	0.8
7300	Melbourne	0.326	0.33	9.8	22	0.4

TABLE 2. Experimental parameters for single-wire spectra traverse experiments.

with overheat ratio set to 1.8. Details of the experimental conditions are given in table 1. The boundary layer thickness (δ) was determined from a Coles law of the wall/wake fit to mean velocity profiles. The friction velocity (U_τ) is obtained from a Clauser chart fit (with log-law constants $\kappa = 0.41$ and $A = 5.0$); U_∞ is the free-stream velocity; l^+ ($= lU_\tau/\nu$) and T^+ ($= tU_\tau^2/\nu$) are the inner-scaled wire length and sample interval respectively. Measurements were made at several wall-normal stations through the log and wake regions. The low Reynolds number measurements were made in an open return suction-type boundary layer wind tunnel of working section $4.7 \times 1.2 \times 0.3$ m (the PIV measurements reported here were made in the same facility: see Hutchins, Hambleton & Marusic 2005b for full details). The higher Reynolds number measurements (from $Re_\tau = 7000$ to 20 000, where $Re_\tau = \delta U_\tau/\nu$) were performed in a separate facility at the University of Melbourne (open return blower-type wind tunnel with working section $27 \times 2 \times 1$ m: see Hafez *et al.* 2004 for full details). The Melbourne experiments were also repeated with a smaller spanwise spacing ($s_y/\delta \approx 0.03$).

In addition to the rake experiments, detailed boundary layer traverses were performed using a single probe across a range of Reynolds numbers in the two facilities. Details of these measurements are given in table 2. Streamwise velocity fluctuations were acquired at logarithmically spaced stations in z, with sufficient sampling frequency to resolve the smallest scales and sufficiently long sample lengths to converge the energy contained in the very largest scales. These data were used to produce the maps of one-dimensional spectra discussed in §6.

3. PIV results

Figure 1 shows sample u fluctuations from various recent PIV measurements made at the University of Minnesota. Plots (a, b and c) are from combined-plane measurements, whereby stereoscopic views of the streamwise/spanwise and streamwise/wall-normal plane are simultaneously acquired (see Hambleton, Hutchins & Marusic 2006 for details). Plot (d) is taken from 45° inclined cross-stream measurements (Hutchins *et al.* 2005b). In all cases the shading shows negative streamwise velocity
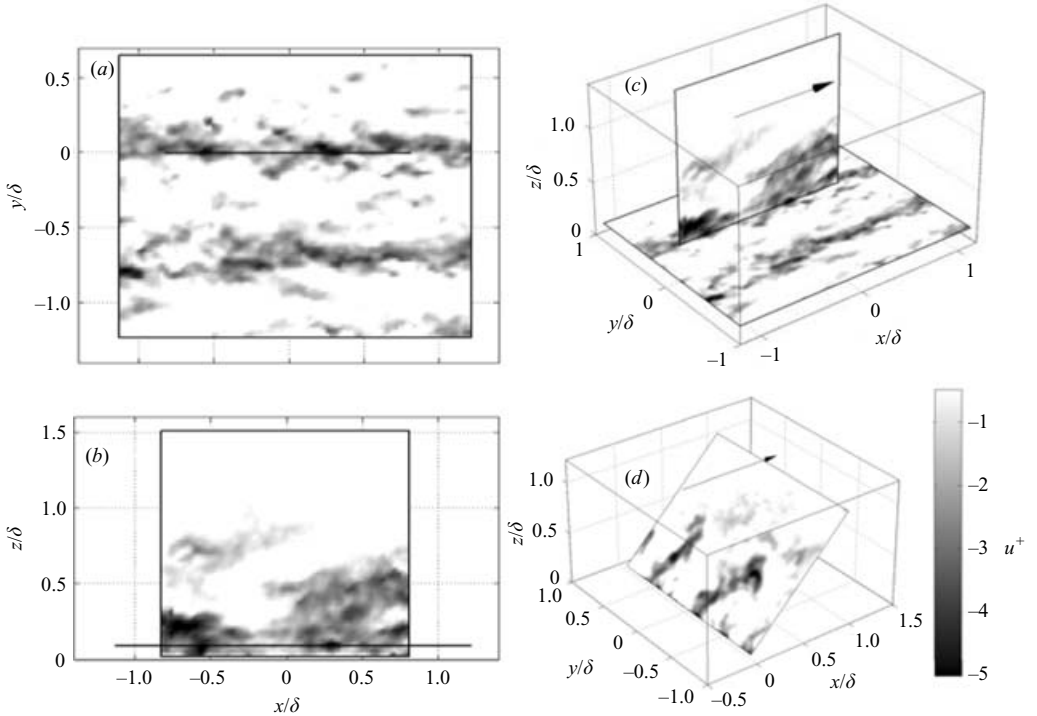
FIGURE 1. Example of instantaneous negative u fluctuations from the combined-plane PIV at $Re_\tau \approx 1100$. (*a*) Plan view showing horizontal plane; (*b*) side view showing vertical plane; (*c*) orthogonal projection showing both planes; (*d*) 45° inclined plane measurement at $Re_\tau \approx 1010$. Thick horizontal lines on plots (*a*) and (*b*) show plane intersects. Grey shading shows negative u fluctuations (see key).

fluctuations (positive fluctuations are set to white). Together these plots illustrate some of the recognized emergent features in the log region. The horizontal plane of figure 1(*a*) clearly exhibits the spanwise stripiness noted by Ganapathisubramani *et al.* (2003) and Tomkins & Adrian (2003). For this log region view ($z/\delta = 0.087$), elongated low-momentum regions persist for the entire streamwise length of the viewing window, with signs of spanwise repetition (Hutchins, Ganapathisubramani & Marusic 2004, 2005*a* analysed spanwise repetition of these large-scale features by notch-filtering the PIV data). The simultaneous side view of plot (*b*) demonstrates that these features have a wider three-dimensional structure, extending some considerable distance in the wall-normal direction. The inclined plane of figure 1(*d*) is not simultaneously acquired, but shows a cross-stream slice through similar features. In this view the previously noted stripiness appears as tall low-momentum eruptions. Vortical structures accompany these low-momentum zones in arrangements that are, in some sense, consistent with the hairpin packet model (noted in various planes by Adrian *et al.* 2000; Tomkins & Adrian 2003; Ganapathisubramani *et al.* 2003; Hutchins *et al.* 2005*b*; Hambleton *et al.* 2006; Marusic & Hutchins 2006). Instantaneous realizations from DNS indicate rather more complex and tangled arrays of vortex cores, yet still clustered in or about these low-speed regions (Tanahashi *et al.* 2004; Jiménez & del Álamo 2004). In all cited cases high momentum fluid has been noted to fill the regions between the low momentum stripes. Together these features dominate the two-point correlations of
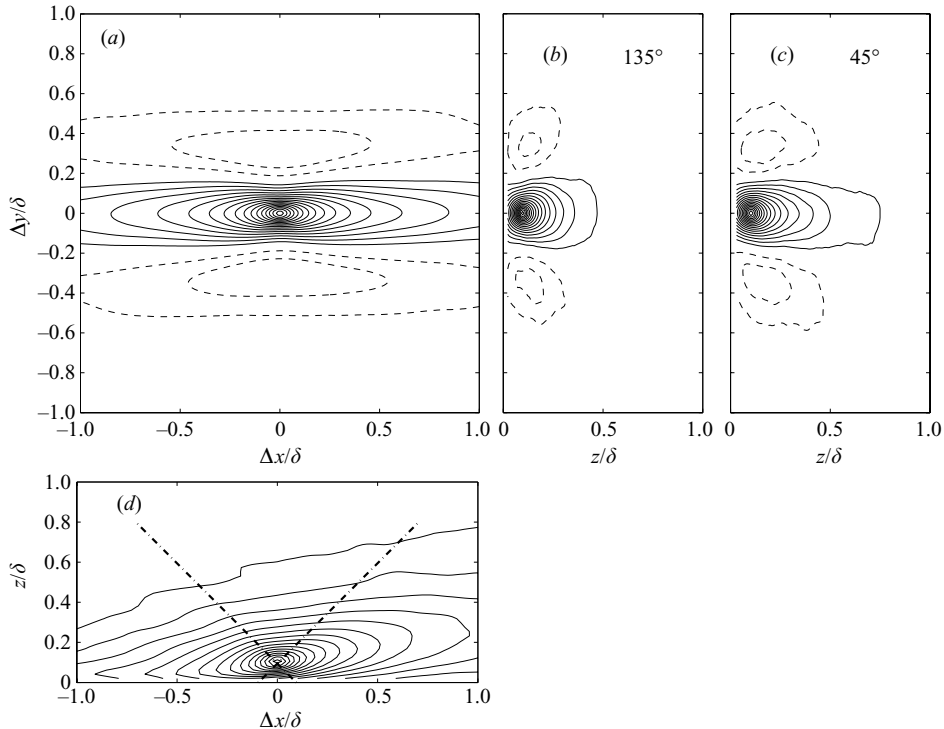
FIGURE 2. Two-point correlations of the streamwise velocity fluctuation R_{uu} calculated at $z_{ref}/\delta = 0.087$ for (a) horizontal and (d) vertical planes from combined plane experiments (b) 135° and (c) 45° inclined plane PIV. Contour levels are from $R_{uu} = -0.12$ to 0.96 in increments of 0.06. Solid lines show positive contours and dashed lines show negative contours.

the streamwise velocity fluctuations (R_{uu}) throughout the log region. Figure 2 shows iso-contours of R_{uu} at $z_{ref}/\delta = 0.087$ (for the same PIV data). Elongated positive correlation regions are flanked in the spanwise direction by anti-correlated behaviour (dashed contours), reflecting the spanwise stripiness of high- and low-momentum regions previously noted in figure 1. It is clear from figure 2(d) and from the 45° and 135° comparison of plots (b) and (c) that the correlated regions are inclined in the downstream direction.

4. Hot-wire rake results

For the instantaneous flow fields and the correlation maps shown above, the length of the log-region structures exceed the PIV field-of-view. The rake measurements were undertaken in an attempt to redress this shortcoming and ascertain the true streamwise length of these features.

4.1. *Two-point correlations*

Figure 3 shows the outer-scaled two-point correlation of streamwise velocity fluctuation, $R_{uu}(\Delta x, \Delta y, z_{ref})$, for the rake experiments. The left-hand side shows the correlations in the streamwise direction at $\Delta y = 0$. This is the autocorrelation, or the streamwise slice at $\Delta y = 0$ through a correlation map of the type shown in figure 2(a). The right-hand side shows the spanwise variation of R_{uu}. For all available Reynolds numbers, spanning well over a decade in Re_τ, there is a good collapse in the outer-scaled R_{uu}. This is all the more striking given the large variation in δ across the
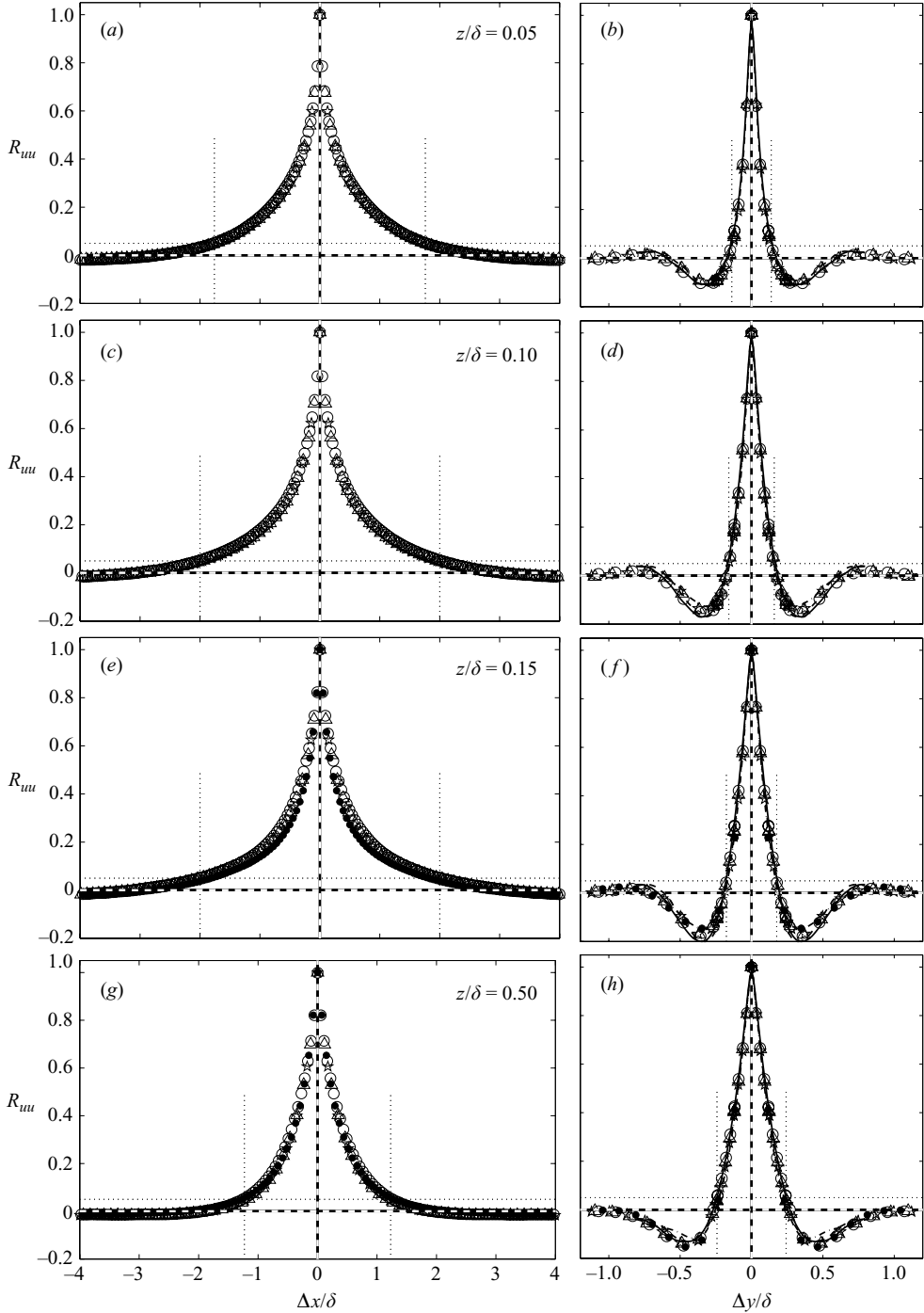
FIGURE 3. Streamwise (left) and spanwise (right) two-point correlations of the streamwise velocity fluctuation R_{uu} calculated at (a, b) $z_{ref}/\delta = 0.05$; (c, d) $z_{ref}/\delta = 0.10$; (e, f) $z_{ref}/\delta = 0.15$; (g, h) $z_{ref}/\delta = 0.50$. Symbols show rake data: (●) $Re_\tau = 1\,120$; (○) $Re_\tau = 7\,610$; (△) $Re_\tau = 14\,380$; (☆) $Re_\tau = 19\,960$. Lines show $45°$ inclined plane PIV results (dash-dotted) $Re_\tau = 1010$; (dashed) $Re_\tau = 1840$; (solid) $Re_\tau = 2800$.
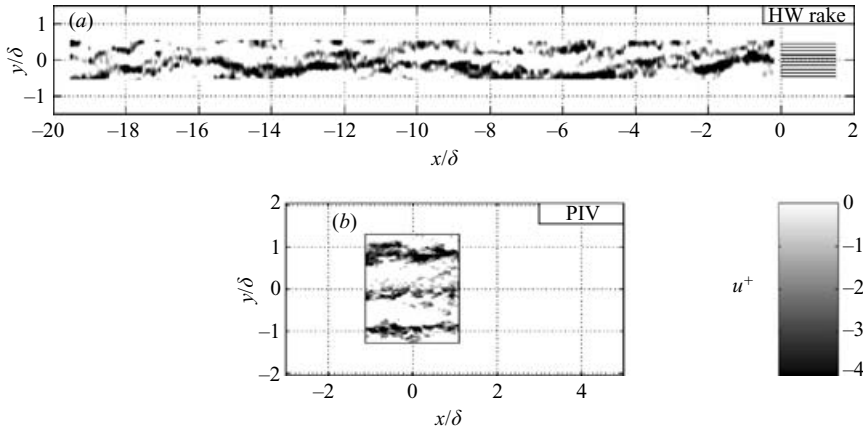
FIGURE 4. (*a*) Example of rake signal at $z/\delta = 0.15$ for $Re_\tau = 14\,380$. The x-axis is reconstructed using Taylor's hypothesis and a convection velocity based on the local mean, $\overline{U} = 15.9\,\mathrm{m\,s}^{-1}$. (*b*) Typical PIV frame for comparison at $Re_\tau = 1100$, $z/\delta = 0.087$. Shading shows only negative u fluctuations (see grey-scale).

experiments (from 0.069 to 0.336 m). Outer scaling of correlation contours in the log and wake regions has also been observed by McLean (1990), Wark *et al.* (1991) and Hutchins *et al.* (2005*b*). The correlation profiles from the inclined plane PIV of Hutchins *et al.* (2005*b*) are included for comparison on the right-hand plots of figure 3. There is some indication of a low Reynolds number effect for the rake and PIV data at Reynolds numbers close to $Re_\tau \approx 1000$. At these Reynolds numbers the streamwise length of the correlations seems to be slightly shorter (solid symbols on figure 3*e*) and the anti-correlated regions seem less pronounced (dot-dashed lines on plots *b*, *d*, *f* and *h*). Certainly at $Re_\tau \sim 1000$ the log region could still be considered as 'developing', with very little scale separation between the near-wall structure and the log region scales.† Regardless, the correlations scale well on boundary layer thickness as we move to higher Re_τ. Comparing the plots on the left-hand side of figure 3 from top to bottom reveals that the streamwise length of the correlations increases from the wall up to the approximate centre of the log region (this length is later shown in §6 to peak at $z/\delta \approx 0.06$), with a pronounced shortening occurring in the outer wake region ($z/\delta = 0.50$). To highlight this effect the dotted lines on figure 3 show the size of the positive correlated regions at $R_{uu} = 0.05$. Considering the right-hand side of figure 3, we note that the spanwise width of the correlation region increases approximately linearly with z/δ for all heights investigated, as was noted for the inclined-plane PIV by Hutchins *et al.* (2005*b*).

4.2. *Instantaneous data*

The streamwise extent of the log region structures has been previously inferred from single-point statistics such as those shown on the left-hand side of figure 3. The long tails in the autocorrelation curves and the peak in the premultiplied spectra $k_x \Phi_{uu}$ have consistently indicated length scales $O(6\delta)$ for turbulent boundary layers. In reality, when raw fluctuating velocity signals from the rake are viewed, we commonly see features that are far in excess of these length scales. Figure 4(*a*) shows a sample

---

† If we take the start of the log region to be $z^+ = 100$ and the upper limit to be $z/\delta = 0.15$, the extent of the log region at $Re_\tau = 1120$ is minimal (spanning only 0.06δ).

segment from the rake at $z/\delta = 0.15$. A very long meandering feature appears to snake through the measurement domain for over 20δ. For the Reynolds number shown ($Re_\tau = 14\,380$) this amounts to a physical length of over 6.5 m. This implies that the log region stripiness previously observed from PIV data is actually a snapshot of a far larger structure (see the PIV comparison in figure 4b). Furthermore, although the low-speed region in figure 4(a) is clearly very long, the meandering tendency will mask its true length from single-point statistics. A synthetic model flow is used in §4.3 to demonstrate this. It should be clarified that the feature shown in figure 4 is by no means unusual and is typical of much of the rake data we have obtained. At the present time it is impossible for us to compile accurate length scale and frequency statistics since, for the most part, these features are rarely fully contained within our measurement domain, and instead tend to wander into and out of our limited spanwise domain due to meandering. All we can really state at this stage is that such events are prevalent features of the log region at all Reynolds numbers we have tested (this is reinforced by the DNS and ASL measurements of §§5 and 7).

4.3. Synthetic flow fields

The log region is modelled with a simple large-scale streak-type structure, consisting of elongated low-speed regions flanked on either side by high-speed regions of similar length and width. The spanwise width of the low- and high-speed regions (L_y) is set to 0.4δ, chosen to reflect the scales observed from instantaneous rake and PIV data (and also the approximate width of the correlation regions in figures 2 and 3). Here we refer to case I as that where the elongated features are perfectly aligned with the mean flow direction, as shown in figure 5(a). Case II corresponds to the same but with an imposed low-frequency spanwise sinusoidal meander, with peak-to-peak amplitude $A = 0.4\delta$ and period $\omega = 12\delta$ (a detailed description of these synthetic flows is given in Appendix A). The entire signal is modulated in the streamwise direction by a Hanning window of length L_x, forcing the fluctuations at either end to zero. Figures 5(a) and 5(b) show the final functions for cases I and II respectively. To create the full synthetic flow fields, the aligned or meandering features are randomly arranged with a normal distribution of length scales, as described in Appendix A.

Figure 5(c) shows the resulting auto-correlation curves for the two cases. Although identical length scales are modelled in each case, the meandering tendency of case II has substantially shortened the length of the positive correlation region. The zero-crossings of the flow-aligned case (solid) approximately reflect the maximum streamwise length of the distributed features. For the meandering case (dashed), the shortened correlation becomes negative at approximately $\Delta x \approx \pm 3.5\delta$, considerably shorter than its true length. Figure 5(d) shows the one-dimensional pre-multiplied streamwise energy spectra in the x direction ($k_x \Phi_{uu}$) for both synthetic flow fields. Once again, it is very clear that the spanwise meandering can lead to a misinterpretation of the true length scale when considering only single-point statistics such as energy spectra.

Additional comments on the potential pitfalls of using energy spectra to infer structural characteristics are further discussed in Appendix B. In the meantime, since we have observed meandering of large-scale features in the instantaneous rake data (figure 4), a more detailed comparison is made with the statistics generated by the meandering synthetic flow field. The anti-correlated regions that occur beyond $\Delta x \approx \pm 3.5\delta$ for the meandering case (II) in figure 5(c) have also been observed in the experimental rake data. Zero-crossings are noted in figure 3(a, c, e), although the resulting regions of anticorrelation are somewhat weaker. The meandering fake
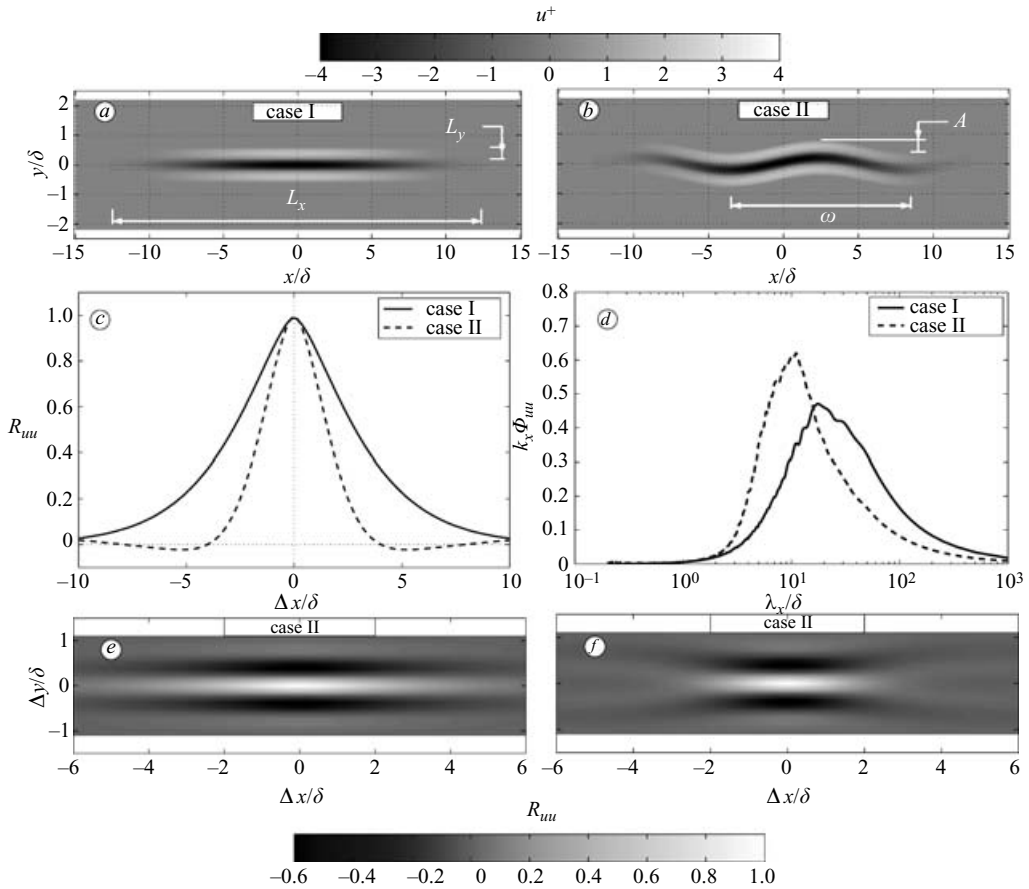
FIGURE 5. The log region modelled as elongated large-scale stripy structures. (*a*) Case I, streamwise-aligned. (*b*) Case II, meandering with amplitude and period of 0.6 and 12δ respectively. Grey scale shows velocity fluctuation (see key). (*c*) Auto-correlations for a random array of each modelled flow. (*d*) Corresponding premultiplied energy spectra (solid) case I; (dashed) case II. The streamwise/spanwise two-point correlation maps of R_{uu} are given for (*e*) case I, (*f*) case II. Grey scale shows R_{uu} level (see key).

features lead to an interesting streamwise/spanwise correlation map beyond the zero-crossing points. These R_{uu} maps are shown for cases I and II in figures 5(*e*) and 5(*f*). As well as being substantially shorter in the streamwise direction, the meandering case (plot *f*) yields a distinctive 'X'-shaped pattern of positive correlation, with anti-correlated regions arranged up- and downstream of the reference point at $\Delta x \gtrsim \pm 3.5\delta$. Interestingly, we see signs of such a pattern when we construct a similar R_{uu} map from the experimental data, shown in figure 6. Though the effect is weaker (the grey-scale increment of figure 6 is altered to highlight this), we note the same distinctive pattern occurring beyond the zero-crossings. The case shown is for the $Re_{\tau} = 14\,380$ experiment at $z/\delta = 0.05$, but these features are evident for all Reynolds numbers and at all measurement heights within the log region. The qualitative similarity between figure 5(*e*) and figure 6 would seem to reinforce our initial observations that the very long features in the log region meander appreciably, and that this hides their true length from single-point statistics.
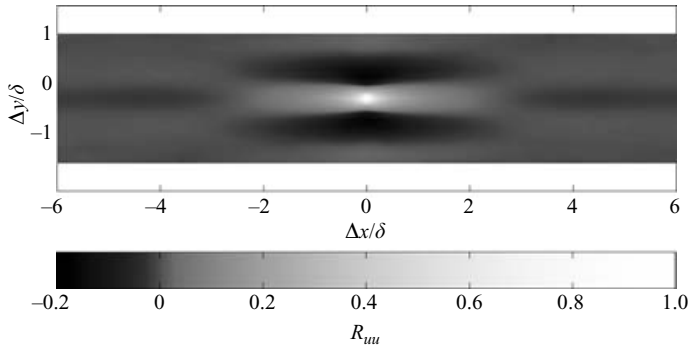
FIGURE 6. Streamwise/spanwise two-point correlation map of R_{uu} at $z/\delta = 0.05$ for $Re_\tau = 14\,380$. Grey-shading shows R_{uu} level (note nonlinear increments: see key).

5. Evidence from direct numerical simulations

Large numerical domain DNS has also uncovered evidence of very large-scale features inhabiting the log region of wall-bounded shear layers. Figure 7 shows streamwise velocity fluctuations from recent channel flow simulations of del Álamo *et al.* (2004) at $Re_\tau = 934$. Plot (*a*) shows the *u* fluctuations in the log region at $z^+ = 150$ ($z/h = 0.164$, where *h* is the channel half-height). Clearly visible in this plot are several occurrences of very long regions of negative *u* fluctuation, visible in the plot as elongated dark regions. (In separate DNS studies Tanahashi *et al.* 2004 show complex clusters of fine-scale vortices existing within these elongated low-speed features.) These features are $>10h$ in length and have characteristic length scales that scale on outer variables (as shown on the earlier correlation plots). For boundary layers, the streamwise and spanwise length scales inferred from the peak in $k_x \Phi_{uu}$ and $k_y \Phi_{uu}$ are of the order $\lambda_x \approx 6\delta$ and $\lambda_y \approx 0.7\delta$ respectively. Different length scales have been reported for channel and pipe flows (Jiménez 1998; Kim & Adrian 1999). Figure 7(*b*) shows the corresponding streamwise velocity fluctuations at $z^+ = 15$ ($z/h = 0.016$). In this near-wall region, inner-scaled streaks dominate with commonly reported characteristic length scales $\lambda_x^+ \approx 1000$ and $\lambda_y^+ \approx 100$ (e.g. Jiménez & del Álamo 2004). As well as illustrating these two scales, figure 7 seems to imply some kind of interaction. If we peer through the small inner-scaled structures of plot (*b*), we can see a faint superimposed footprint of the larger-scale features. This characteristic is highlighted by applying a filter of size ($h/2 \times h/2$) to both planes of data. Here, the aim of the filter is to average away the small-scale features, and for this purpose a simple Gaussian is adequate. Figure 7(*c*) and (*d*) shows just the negative streamwise velocity fluctuations as grey-scale contours for the filtered fields, and it is noted that remarkable similarities now appear between the remaining large-scale events for both wall-normal positions. One such feature is highlighted by the dot-dashed contour on figure 7(*c*), which is drawn at a small negative value ($u^+ = -0.2$). This feature exceeds the length of the numerical domain ($>25h$). When the same contour is plotted on figure 7(*d*), with an appropriate streamwise shift, we note that it encloses almost exactly the same large-scale feature. If we refer back to the original velocity fields of plots (*a*) and (*b*) it is possible to discern this large-scale feature even through the unfiltered data. In separate DNS studies, Abe, Kawamura & Choi (2004) have also noted a footprint from the outer-layer structure onto the near-wall region, observing that these large-scale structures contribute to the shear-stress fluctuations. Tsubokura (2005) concluded a similar result from LES studies of
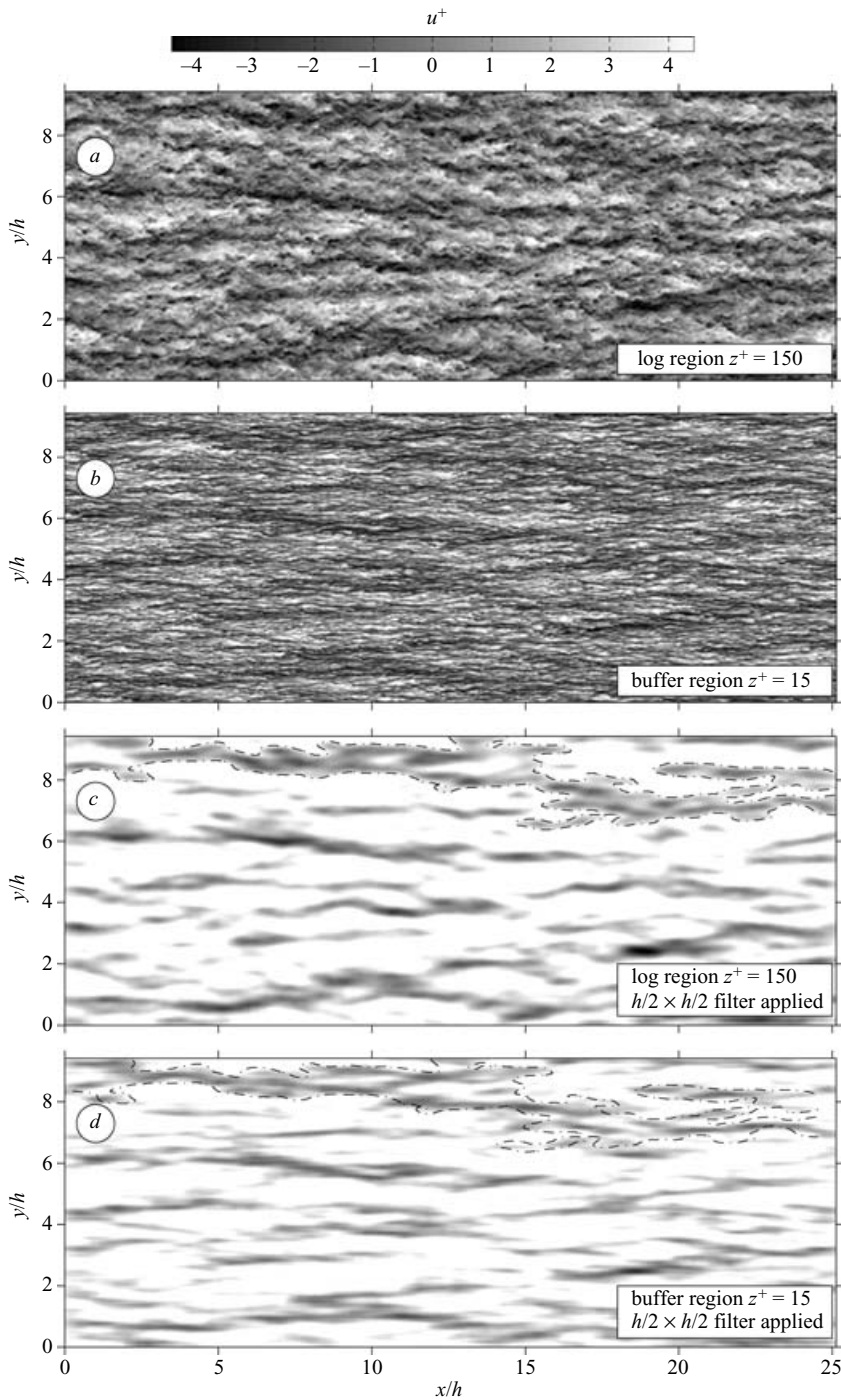
FIGURE 7. Instantaneous flow fields from $Re_\tau = 934$ channel simulations (del Álamo *et al.* 2004). Shading shows u fluctuations (*a*) at $z^+ = 150$; (*b*) at $z^+ = 15$ (see upper grey-scale). Plots (*c*) and (*d*) show the filtered data at the same respective heights (shading shows negative u fluctuations, grey-scale as figure 4).

pipe and channel flows. Hutchins *et al.* (2005*b*) have shown previously that the large-scale log and wake region events retain a measurable correlation with the near-wall buffer region ('attached' and 'detached' correlation regimes), and by such mechanisms very low wavenumber energy leaches into the near-wall region. This conclusion is well supported by the result in figure 7, and is consistent with the finding that the streamwise turbulence intensity in the viscous sublayer and buffer region will have a δ-scale influence (see for example DeGraaff & Eaton 2000; Metzger *et al.* 2001; Metzger & Klewicki 2001; Marusic & Kunkel 2003; Jiménez, del Álamo & Flores 2004). Further implications to Reynolds number scaling will be considered in §6.

   The mechanisms that give rise to the large-scale features in the log region are somewhat unclear at this stage. Figure 7(*b*) seems to show that the small inner-scaled near-wall features are arranged into larger outer-scaled agglomerations, possibly by the footprint of the log region structures. We should not, however, exclude the possibility that there is a feedback mechanism by which the modulated near-wall events influence the large-scale structures (although such scenarios become increasingly difficult to countenance at high Reynolds number, where the separation in scale between these inner- and outer-scaled events becomes very large see §7). The autonomous channel simulations of Jiménez *et al.* (2004) would seem to imply that the near-wall structures can self-organize into very long features even in the absence of the outer scales, and Jiménez & del Álamo (2004) attribute the very long *u* fluctuations in the log region to 'passive wakes' formed downstream of smaller attached clusters of vortices originating from the buffer region. They suggest that these 'wakes' spread under the effect of background turbulence. However, it is worth noting that a similar-looking 'spreading wake' can be obtained by conditionally averaging on meandering features such as those shown in figure 5. Furthermore, in an instantaneous sense, neither the PIV nor the DNS data exhibit any signs of a widening of these large-scale features in the streamwise direction (see figures 1*b*, 4*a* and 7*a*†). In further DNS studies, Toh & Itano (2005) also note near-wall scales existing under large-scale structures and suggest that these two disparate scales interact in a co-supporting cycle. Certainly, figure 7 implies a connection between the two scales. As a final important point, the authors have recently noted that the very long log region structures exist even over fully roughened walls, which would imply that the near-wall cycle is not responsible for their formation.

6. Reynolds number effects

   It is now well known that the inner-scaled peak in the streamwise turbulence intensity rises with Reynolds number. One of the first clear examples of this is given by DeGraaff & Eaton (2000) and Metzger & Klewicki (2001), who collated streamwise turbulence intensity results from hot-wire measurements where the non-dimensional wire length was less than 10 wall units (to avoid any possibility of spatial resolution issues). The collated results convincingly demonstrate that the peak rises with Reynolds number. Since that time, similar results have been presented by Marusic & Kunkel (2003) and Jiménez & del Álamo (2004). Figure 8 replots the data from Metzger & Klewicki (2001), with the addition of numerical results and the similarity approximations of Marusic & Kunkel (2003). In general, figure 8

---

† If there were substantive widening of flow features in the streamwise direction, it would be simple to deduce flow direction without reference to the axis system in the streamwise/spanwise planes of figures 1(*b*), 4(*a*) and 7(*a*). This is not the case (flow is from left to right).
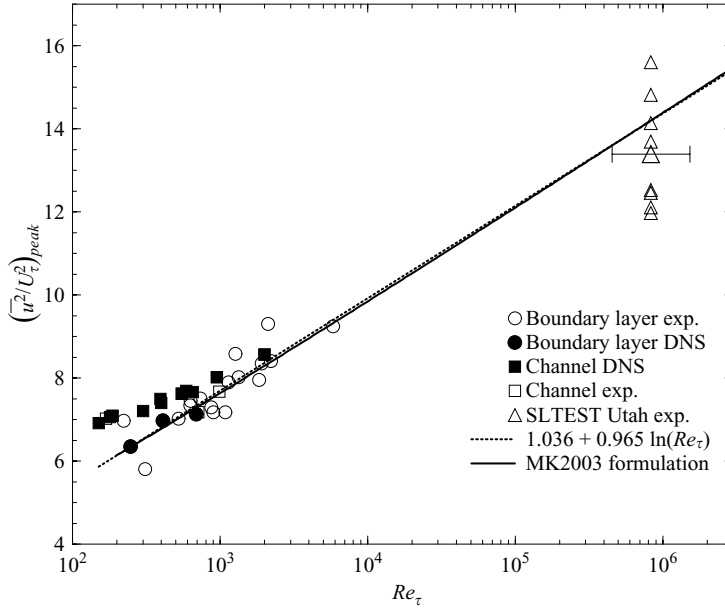
Authors	Re_τ	Flow	Technique
DeGraaff & Eaton (2000)	734, 1335, 2217, 5813	BL	exp
Ueda & Hinze (1975)	633, 1918	BL	exp
Ligrani & Bradshaw (1987)	1140	BL	exp
Balint *et al.* (1991)	1088	BL	exp
Johansson *et al.* (1987)	1845	BL	exp
Johansson & Karlsson (1989)	900	BL	exp
Ching *et al.* (1995)	222, 627	BL	exp
Purtell *et al.* (1981)	311, 870	BL	exp
?	522, 1269, 2109	BL	exp
Spalart (1988)	248, 410, 690	BL	DNS
Wei & Willmarth (1989)	169, 714, 989	CH	exp
Jiménez and coworkers	186, 547, 934, 2003	CH	DNS
Moser *et al.* (1999)	180, 395, 590	CH	DNS
Iwamoto *et al.* (2002)	110, 150, 300, 400, 650	CH	DNS
Metzger & Klewicki (2001)	8×10^5	ASL	exp (SLTEST)

FIGURE 8. Variation of the peak value of the inner-scaled streamwise turbulence intensity with Reynolds number (around $z^+ \approx 15$). $\square$, channel flow; $\bigcirc$, boundary layer; $\triangle$, atmospheric surface layer. Solid symbols are DNS results, open are experimental. MK2003 refers to Marusic & Kunkel (2003).

reinforces the same trend with Reynolds number, although there is some suggestion that channel flows (square symbols) may behave differently to boundary layers at the low Reynolds number end. The dashed line shows the similarity approximation of Marusic & Kunkel (2003), which describes well the available boundary layer data. A simple curve fit to their result is given by

$$\left(\frac{\overline{u^2}}{U_\tau^2}\right)_{peak} = 1.036 + 0.965 \ln(Re_\tau). \tag{6.1}$$

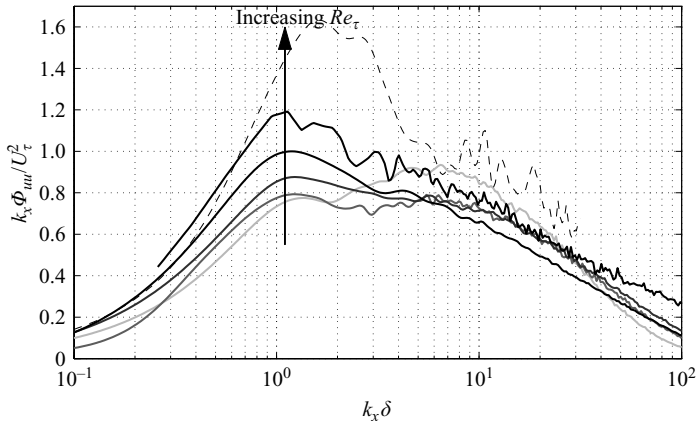FIGURE 9. Pre-multiplied energy spectra $k_x \Phi_{uu}/U_\tau^2$ at $z/\delta = 0.06$ for laboratory hot-wire measurements. Line shading indicates Reynolds number. From lightest to darkest $Re_\tau = 1010$, 1910, 2630, 4110 and 7300. Dashed line shows sonic anemometer data from SLTEST (Utah 2005) at $Re_\tau \approx 6.6 \times 10^5$, $z/\delta = 0.06$.

By low-pass-filtering the high Reynolds number data, Metzger & Klewicki (2001) show that the additional energy in the near-wall streamwise velocity fluctuations comes from low-wavenumber events. Figure 7 clearly shows the origins of the low-wavenumber energy, which is present in the near-wall region in the form of a footprint from the very large outer-scaled log-region structures. In order to consider the scaling of the low-wavenumber contributions, figure 9 shows pre-multiplied spectra scaled with U_τ^2 ($k_x \Phi_{uu}/U_\tau^2$) for various laboratory hot-wire measurements at $z/\delta = 0.06$, made in the range $1010 \leqslant Re_\tau \leqslant 7300$ (experiments are described in §2 and table 2). For these data it is noted that a strengthening peak emerges in the pre-multiplied spectra with Reynolds number, centred around $k_x \delta \approx 1$, and increasing in magnitude with Re_τ. Clearly a Reynolds number dependence is evident, indicating that the large-scale structures in the log region may not scale exclusively on U_τ. If it can be established that the large-scale structures are caused by the local shear in the log region then the velocity difference across this region might be a suitable candidate. However, this remains unclear and further study is required to resolve the velocity scaling issue for the largest structures. In particular, high Reynolds number data are needed to confirm the trend with increasing Re_τ. As an example, a preliminary result from the atmospheric surface layer is included in figure 9 as a dashed line. Though this indicates a continuing Re_τ dependency, some caution is required owing to uncertainty over convergence. This measurement was obtained from 1 hour of sonic anemometer data during periods of steady wind and neutral buoyancy on 2 June 2005 (see §7).

To gain a better insight into the contributions to the u spectra across the boundary layer, figure 10 shows colour contours of $k_x \Phi_{uu}/U_\tau^2$ versus $\log(\lambda_x/\delta)$ across all measured wall-normal positions, together with the corresponding mean velocity and turbulence intensity profiles. Plots (a) to (d) represent increasing Reynolds number, with $Re_\tau = 1010$, 1910, 2630 and 7300 respectively. The figure shows two distinct energy peaks emerging with increasing Reynolds number. For convenience we will refer to these as the 'inner' and 'outer' sites. The inner site is fixed in viscous coordinates, occurring at $z^+ \approx 15$ and $\lambda_x^+ \approx 1000$ (shown by the white + symbol). For the Reynolds numbers shown here this is the strongest peak, and occurs at the same wall-normal location as the peak in the broadband turbulence intensity (shown by the filled circles).
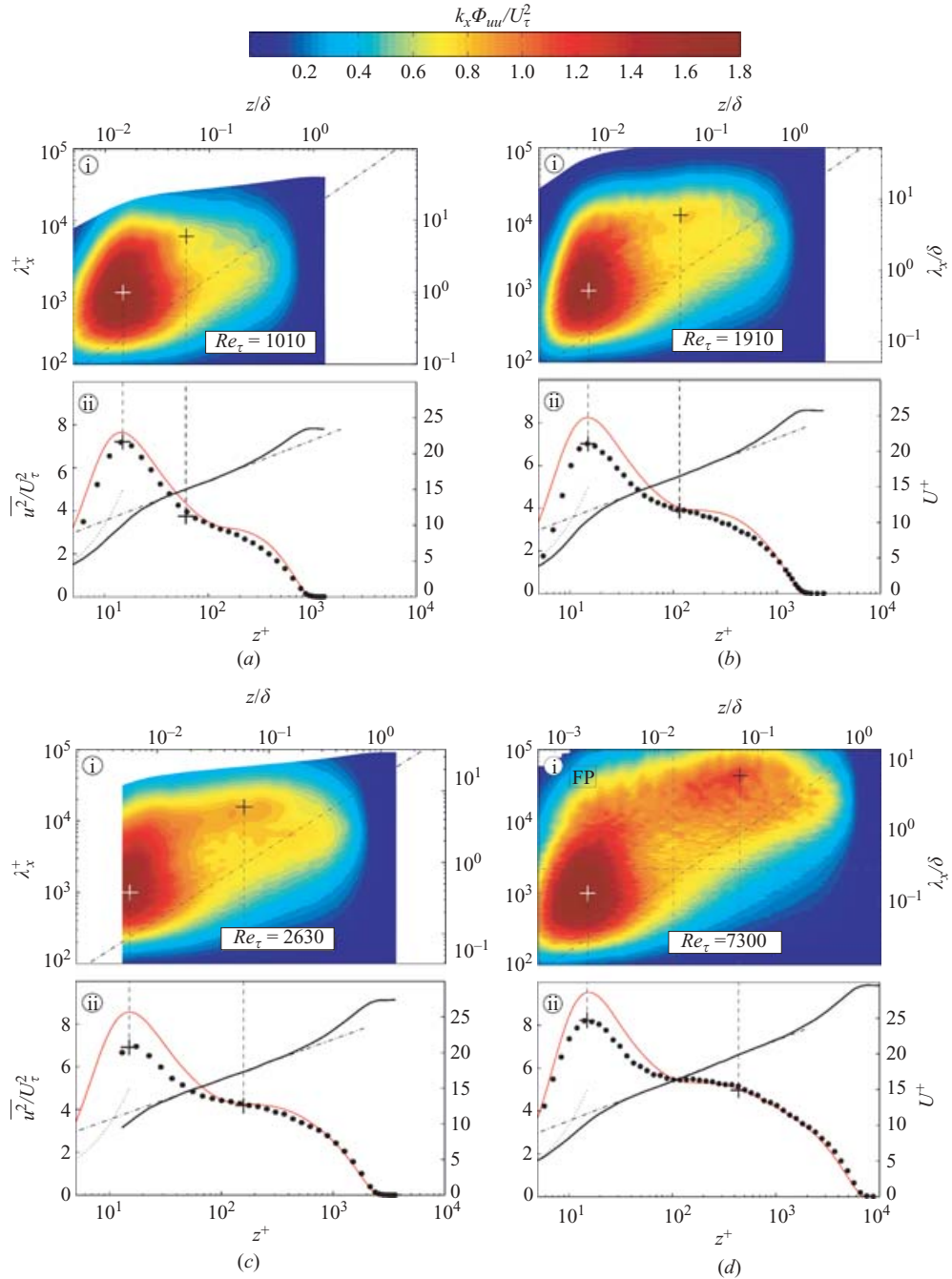
FIGURE 10. (i) Contour maps showing variation of one-dimensional pre-multiplied spectra with wall-normal position for (*a*) $Re_\tau = 1010$; (*b*) $Re_\tau = 1910$; (*c*) $Re_\tau = 2630$; (*d*) $Re_\tau = 7300$. The *y*-axis shows length scale in both inner (left) and outer (right) scaling. The *x*-axis shows wall-normal position for both inner (lower) and outer scaling (upper). The colour scale shows magnitude of $k_x\Phi_{uu}/U_\tau^2$. (+) denote 'inner' and 'outer' energy sites (white) $\lambda_x^+ = 1000$, $z^+ = 15$ and (black) $\lambda_x = 6\delta$, $z = 0.06\delta$. Dot-dashed lines show k_x^{-1} limits $\lambda_x = 15.7z$ (and $z^+ = 100$ and $\lambda_x = 0.3\delta$ for plot *d*). (ii) Corresponding mean profiles of (●) turbulence intensities and (−) velocity. Dotted line shows $u^+ = z^+$. Dashed lines and (+) symbols denote $z^+ = 15$ and $z = 0.06\delta$. Dot-dashed line shows $U^+ = (1/\kappa)\ln(z^+) + A$ (where $\kappa = 0.41$ and $A = 5.0$). Red line shows MK2003 formulation.

This inner site is due to the near-wall cycle of streaks and quasi-streamwise vortices (Kline *et al.* 1967; Jiménez & Pinelli 1999; Schoppa & Hussain 2002). As Reynolds number increases, the second (outer) energy site emerges (shown by the black + in figure 10). This occurs within the logarithmic region of the mean velocity profile and is approximately fixed in outer coordinates at $z/\delta \approx 0.06$ and $\lambda_x/\delta \approx 6$ (although there is some indication that the precise location of the peak wanders gradually with Reynolds number). The energy in this outer site comes from the largest modes in the turbulent boundary layer that we have here termed 'superstructures'. Namely, the very long regions of meandering positive and negative u fluctuation inhabiting the logarithmic region, as evidenced by the PIV, hot-wire rake and DNS data of figures 1, 4 and 7 respectively. The size of these events scales on δ, and their magnitude primarily on U_τ^2 but with a clear Re_τ dependence. A cursory glance at the increasing Reynolds number cases of plots (*a*) to (*d*) gives a very vivid impression of the emergence of the outer energy site with Re_τ. At the lowest Reynolds number, there is insufficient separation of scales to observe the outer peak and the energy from the inner-scaled events swamps the weaker log region structure. The plots indicate that Reynolds numbers of $Re_\tau \gtrsim 2000$ are required before we will clearly see an emergence of the outer site. It is also important to note from the higher Reynolds number cases of figure 10 that the emergent large-scale energy is felt all the way down to the wall (this region is labelled FP for footprint in figure 10*d*). This increasing presence of low-wavenumber energy in the near-wall region will likely contribute to the rising near-wall peak in the broadband turbulence intensity at $z^+ = 15$ (see figure 8). The low-wavenumber energy is essentially the footprint due to the log region structure imparting a large-scale organization or modulation on to the near-wall cycle (see figure 7). Del Álamo & Jiménez (2003) decomposed u fluctuations from $Re_\tau = 550$ channel DNS into two plots of $k_x \Phi_{uu}$ where $\lambda_y > 0.75h$ and $\lambda_y < 0.75h$. They show similar trends of inner and outer energy sites to those shown in figure 10 (although to see this behaviour at low Reynolds numbers required segregation according to spanwise scale).

It is important to monitor the effect of limited spatial resolution for the spectra shown in figures 9 and 10. The same hot-wire probe was used for all Minnesota spectra and thus the non-dimensional wire length has varied from $l^+ = 14$, 30, 40 and 67 for $Re_\tau = 1010$, 1910, 2650 and 4110 (see table 2). This can clearly be seen in the diminishing magnitude of the inner energy site in figure 10(*a–c*) at $z^+ \approx 15$, $\lambda_x^+ \approx 1000$. The $Re_\tau = 7300$ measurements were made in a larger facility and are better resolved with $l^+ = 22$. For the results reported here, spatial resolution is not such an issue when considering the large-scale low-wavenumber phenomena in the logarithmic region of the boundary layer (figure 9). However, in the near-wall region, where the energy-contributing motions are smaller, the limited resolution becomes a problem. The red lines on the profile plots of figure 10(ii) show the predicted turbulent intensities for each Reynolds number and thus highlight the discrepancies. These lines are from the similarity formulation of Marusic & Kunkel (2003), which has been shown to compare well to other high spatial resolution data at these Reynolds numbers (such as those shown in figure 8).

From scaling arguments based on the attached eddy hypothesis (Townsend 1956; Perry, Henbest & Chong 1986; Marusic & Perry 1995) we would expect to see k_x^{-1} behaviour spanning the region between the inner and outer energy sites for eddies that scale with their distance from the wall. A hairpin vortex packet scenario would be consistent with these attached eddies being mainly aligned and spatially arranged within the large superstructure (Marusic 2001), which is also consistent with VLSM of Kim & Adrian (1999). Owing to the presence of the aforementioned inner and

outer energy sites, significant regions of k_x^{-1} behaviour are only possible for high Reynolds numbers very close to the wall. Nickels *et al.* (2005) estimated that a k_x^{-1} region in the *u*-spectra will occur within the limits $k_x \delta > 21; k_x z < 0.4$ for $z^+ > 100$. Therefore a triangular k_x^{-1} region would appear as a plateau on the premultiplied spectra plots in figure 10 bounded by

$$z^+ > 100, \quad \lambda_x/z > 15.7, \quad \text{and} \quad \lambda_x/\delta < 0.3.$$

Based on the above limits the k_x^{-1} region will not exist for $Re_\tau < 5230$, and thus it is only on figure 10(*d*) at $Re_\tau = 7300$ that a small k_x^{-1} region appears. Even so, with increasing Reynolds number it is clear that the intermediate scales (between the inner and outer energy sites) in the log region do tend to follow the trend described by the k_x^{-1} formulation (the line $\lambda_x/z = 15.7$ is shown on each spectra plot in figure 10). Further high Reynolds number experimental data are needed to confirm this behaviour fully. Such experiments are also required to remove any uncertainty regarding the apparent strengthening of the 'superstructures' with increasing Re_τ, as suggested by the data in figure 9. In this case the extent of a k_x^{-1} region would be further reduced as the outer energy site encroaches on the limit $\lambda_x/\delta = 0.3$.

Figure 11 is a sketch summarizing our interpretation of some salient features of the spectra shown in figure 10. In this simple model, the energy spectrum is composed of two main separate energy sites. Close to the wall, at the point of maximum turbulence production, the near-wall cycle causes an inner energy site with location and magnitude fixed in viscous units (ν and U_τ). In the logarithmic region the 'superstructures' lead to an outer energy site with location fixed on outer units (δ) and a magnitude that appears to rise with Reynolds number. As Re_τ increases, these two sites become increasingly separated. Co-existent in the logarithmic region is a region of k_x^{-1} behaviour due to attached eddies that scale with distance from the wall z and U_τ. In addition, and not shown on figure 11, we would expect wake structure contributions beyond the edge of the logarithmic region due to eddies that scale with δ and U_τ (Perry & Marusic 1995), although their contribution is relatively weak in zero pressure gradient flows.

Examples of the structure associated with inner and outer energy sites are included in figure 11 as grey-level contours of *u* fluctuation. The data are from the channel flow DNS of del Álamo *et al.* (2004) and are included for illustrative purposes only. (The sketched spectrum corresponds to $Re_\tau \approx 4000$, while the DNS data are for $Re_\tau = 934$.) These data highlight the inner/outer interaction, with energy from the outer site or 'superstructure' extending down to the near-wall region. This is evident in both the spectrum and the two *x*-*y* planes of *u* fluctuation, where the large-scale structure in the log region leaves a faint imprint on the near-wall region. The white contour highlights the same large-scale feature evident at both wall-normal locations (a large low-speed, darker-shaded region). The contribution of this footprint to the energy spectrum is shown by the arrows linking these two contours. As Reynolds number increases, the footprint in the near-wall region will become progressively more noticeable. This is not only due to the increasing scale separation between the inner and outer scales, but also because the magnitude of the 'superstructure' fluctuation becomes increasingly comparable to the (viscous-scaled) fluctuation due to the near-wall cycle.

As noted earlier, all the above is consistent with a need for both inner and outer scaling for the streamwise turbulence intensities in the near-wall region. The arguments would also apply to the spanwise turbulence intensities ($\overline{v^2}/U_\tau^2$) but not to the wall-normal intensities ($\overline{w^2}/U_\tau^2$) and the Reynolds shear stress ($-\overline{uw}/U_\tau^2$) owing to the
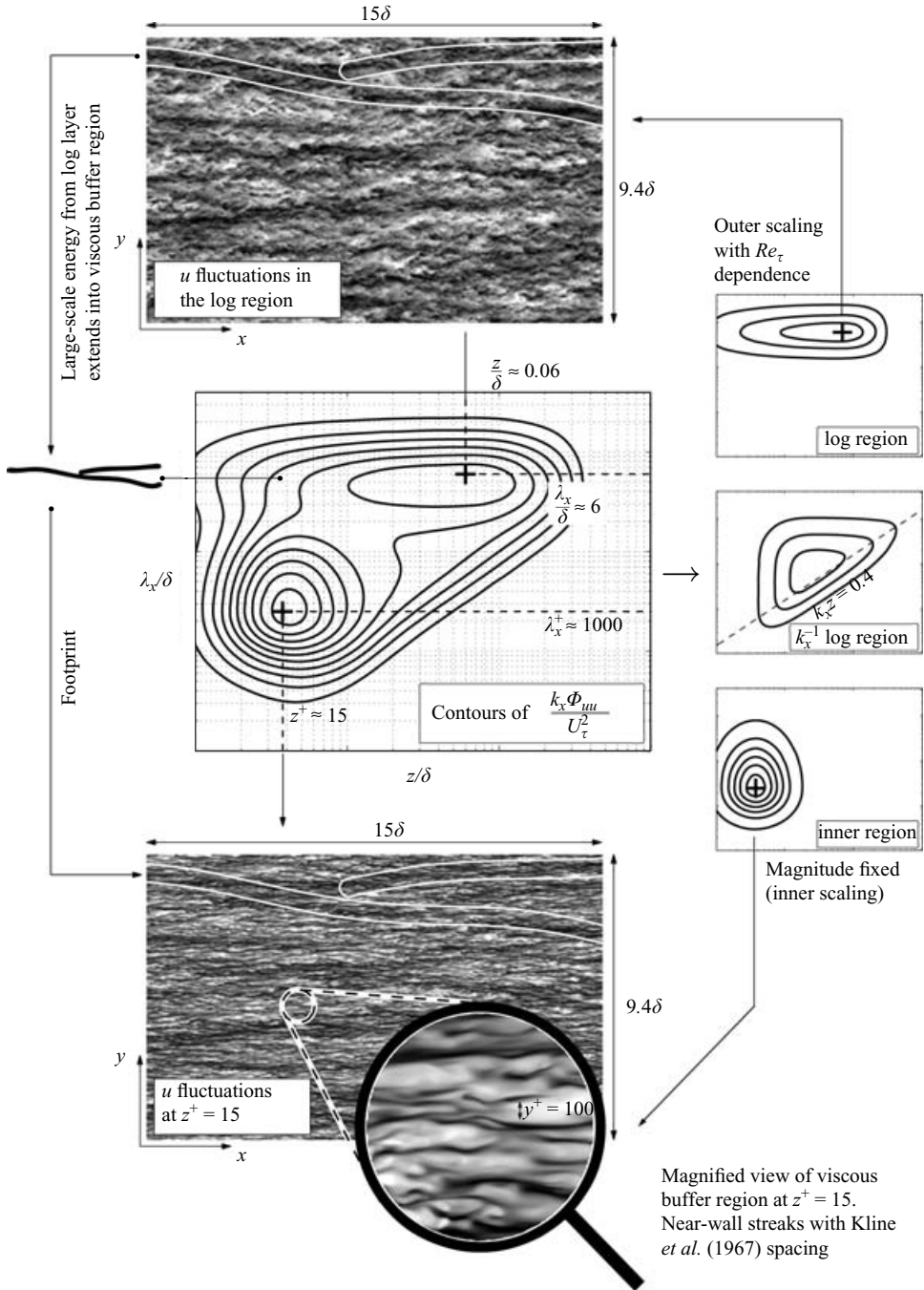
FIGURE 11. Schematic explaining the relative contributions to the energy spectra shown in figure 10. The main iso-contour plot has three salient components, as shown on the right-hand side.

blocking effect of the wall. (Within vortex-based models, one can also interpret this blocking effect as the image vortex structures in the wall.) Certainly this is reflected in experimental and DNS data by a spatial compactness of w and Reynolds stress

fluctuations as compared to u and v (Ganapathisubramani *et al.* 2003, 2005; Hoyas & Jiménez 2006). However, an important fact that is often overlooked in these statistics is that although w and uw do not contain energy at low wavenumbers, the individual spatially compact concentrations exhibit a strong alignment with the extremely long u modes of the superstructure (see Ganapathisubramani *et al.* 2003 and Marusic & Hutchins 2006 for examples of this, and all literature pertaining to hairpin packet models).

Evidence of an outer-scale contribution to the near-wall region is not new, and has been noted in the literature for many decades. One particular study is that of Rao, Narasimha & Badri Narayanan (1971), who considered scaling of the near-wall 'bursting' frequency. Using only single-point time-series data, they were able to deduce that large outer-scaled structures were active in rearranging and interacting with the near-wall structure. This is basically the same conclusion that we arrive at from our study.

7. The atmospheric surface layer (ASL)

Preliminary results from recent experiments performed in the atmospheric surface layer will also be briefly discussed. These data make a useful high Reynolds number appendix to the preceding discussion. Experiments were conducted at the SLTEST facility, located in Dugway Proving Grounds, Utah. Full details of the facility are available in Klewicki *et al.* (1995), Metzger & Klewicki (2001) and Kunkel & Marusic (2006). The unique geography of this site enables measurements to be made in extremely high Reynolds number turbulent boundary layers ($Re_\tau \approx O(10^6)$) that have developed over 100 km of low surface roughness featureless salt flat (equivalent sand grain roughness $k^+ \approx 22$). These atmospheric measurements are essentially a scaled-up version of the hot-wire rake experiments described in §2, with wall-normal position and spanwise separation scaled on the expected boundary layer thickness (δ is estimated at 60 m for the ASL). A spanwise array of 10 sonic anemometers (Campbell Scientific CSAT3) are deployed on tripods mounted 2.14 m above the desert floor and spaced 3 m apart in the spanwise direction. At one end of the spanwise array is located an additional wall-normal array of 9 logarithmically spaced sonic anemometers (from $z = 1.4$ to 25.7 m). A photograph of the measurement array installed at the SLTEST site is included here as figure 12. Details of the experimental procedure will be reported in full elsewhere.

We will consider an hour of data taken from a period of neutral buoyancy and steady wind conditions during the early hours of 2 June 2005. Mean statistics from this hour compare well to canonical turbulent boundary layers measured in laboratory facilities. The mean velocity profile obtained from the wall-normal array is logarithmic, which together with U_τ indicates that the log-law extends from 9 mm above the wall to beyond the top of the tower (the entire tower shown in figure 12 is located within the log region). Turbulent intensities are as predicted by the similarity approximations of Marusic & Kunkel (2003). Spanwise correlations of streamwise velocity fluctuation (R_{uu}) for the spanwise array are shown in figure 13 and compare well to the correlations measured with the hot-wire rake (see §4.1). The symbols show the correlation data from laboratory measurements across the Reynolds number range $1840 < Re_\tau < 19960$. The solid lines show the corresponding data for the hour of ASL data. The collapse with outer scaling is remarkably good, especially considering that the comparison between the symbols and the lines represents a Reynolds number range of more than two decades (and δ has varied by three orders of magnitude).
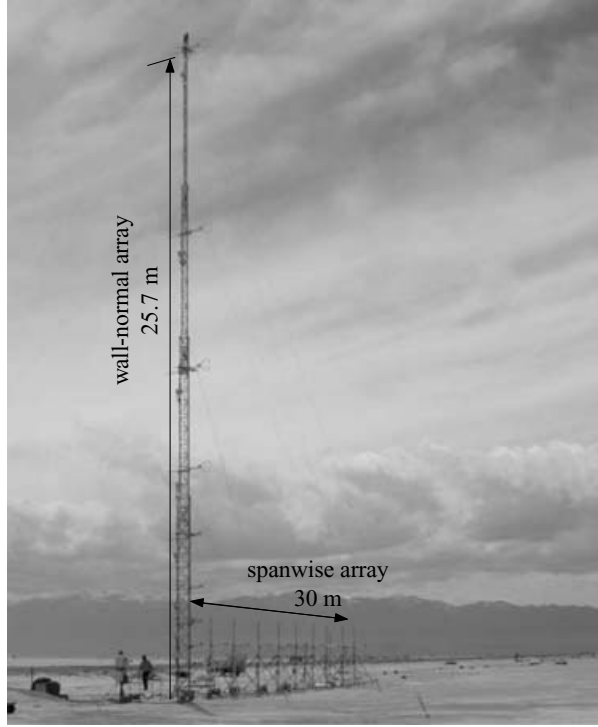
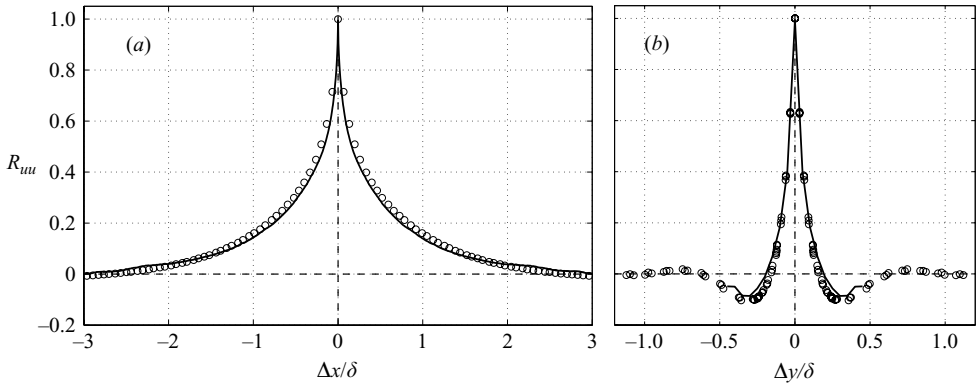FIGURE 12. View of the measurement array installed at the SLTEST site.

FIGURE 13. (*a*) Streamwise and (*b*) spanwise two-point correlations of the streamwise velocity fluctuation R_{uu}. ($\bigcirc$) show rake data for $1840 < Re_\tau < 19960$ at $z/\delta = 0.05$; solid line shows Utah data for $Re_\tau \approx 660000$ at $z/\delta = 0.036$.

There are some signs that the ASL correlations are not fully converged. Even with one hour of data, the total advection length for the ASL measurement is only approximately 300δ as compared to over 37000δ for the $Re_\tau = 19960$ laboratory data. Convergence of low-wavenumber information will always be problematic in atmospheric measurements owing to limited periods of neutral stability and very large structural length scales. Regardless, figure 13 shows that similar large-scale features inhabit the log region of high Reynolds number atmospheric surface layers. The long region of positive correlation, flanked in the spanwise direction by anti-correlated
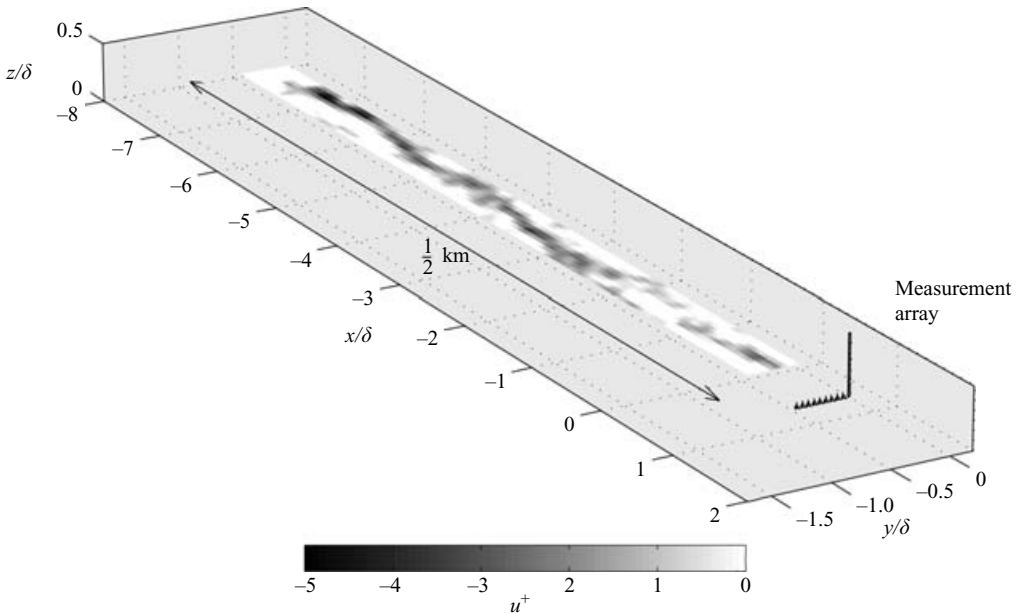
FIGURE 14. Example of signal across the spanwise array of sonic anemometers at SLTEST, $z/\delta = 0.037$, $Re_\tau = 660\,000$. The x-axis is reconstructed using Taylor's hypothesis and a convection velocity based on the local mean, $\overline{U} = 5.46\,\mathrm{m\,s}^{-1}$. Shading shows only negative u fluctuations (see grey scale).

behaviour is a typical statistical signature of the 'superstructure'. Figure 14 shows instantaneous streamwise velocity fluctuations for a 100 s trace across the spanwise array. The streamwise ordinate is reconstructed using Taylor's hypothesis, in exactly the same way as for figure 4. It is immediately obvious that the same very long meandering features inhabit the log region of the ASL. The feature shown in figure 14 is almost half a kilometre in length. Some sense of proportion can be obtained from the schematic of the measurement array, which is drawn to scale on the figure (compare to the photograph in figure 12). A comparison with laboratory results would indicate that even longer features will occur ($>20\delta$). Indeed, the meandering tendency of these large-scale features means that they often wander into and out of our measurement domain before we can assess their true length (the spanwise width of the sonic anemometer array is only 0.5δ and the sample length is also somewhat limited).

The feature shown in figure 4 is enormous in comparison to the near-wall structure (1000 wall units in the ASL equates to 90 mm). With this kind of scale separation between the near-wall cycle and the log region structure, it becomes increasingly less intuitive to sanction a situation whereby the near-wall cycle can influence or give rise to the 'superstructure'. Certainly at lower Reynolds number the degree of scale-overlap tends to give the impression that these two scales are intimately entwined. Perhaps this is so at low Reynolds numbers, with the log region structure subject to a certain degree of wall-up interaction from the near-wall cycle. However, for the ASL, we are left with the notion that the inner and outer energy site (figure 11) could be two quite separate regimes, and that any substantial interaction is likely to be top-down (Hunt & Morrison 2000). Circumstantial evidence for this scenario comes from Jiménez & Pinelli (1999), who demonstrate that the near-wall cycle is autonomous and can

continue largely unabated even in the absence of external (large-scale) influence. In addition, the existence of 'superstructure'-type features over fully roughened walls (where the near-wall cycle in theory no longer exists) implies that the log region structure is shear-driven rather than relying on a specific near-wall formation process.

8. Conclusions

The principle findings of this study are summarized by the following points.

(i) *Superstructures*. hot-wire rake measurements have confirmed that very long meandering features populate the log region of turbulent boundary layers, extending to over 20δ in length. These features form the stripiness noted in PIV experiments that has been previously related to the hairpin packet paradigm and shown to carry a large proportion of the Reynolds shear stress in the log region (Ganapathisubramani *et al.* 2003; Marusic & Hutchins 2006). These may be what Kim & Adrian (1999) referred to as *very large-scale motions* (VLSM) in turbulent pipe flow.

(ii) *Outer scaling*. the superstructures have a dimension that scales on boundary layer thickness δ. Thus as Reynolds number increases they become increasingly large in comparison to the near-wall structure. Taking the inner and outer characteristic length scales from the local peaks in the pre-multiplied energy spectrum of u (figure 10), we can approximate that the superstructure is larger than the near-wall structure by a factor of at least $6Re_\tau/1000$. The streamwise velocity fluctuations due to the superstructures appear to be Reynolds number-dependent. Further studies, including higher Reynolds number data, are likely required to fully determine their correct velocity scale.

(iii) *Meandering*. instantaneous views of u fluctuation in the log region suggest that the superstructure meanders substantially along its length (see hot-wire rake, DNS and sonic anemometer data of figures 4, 7 and 14). By studying synthetic meandering flow features, it is shown that this meandering can severely curtail the length scales we infer from two-point correlations and pre-multiplied energy spectra (§ 4.3). The fact that longer length scales are reported in the log region of pipe flows than for boundary layers (Kim & Adrian 1999) may suggest that spanwise (or azimuthal) meandering is to some degree constrained in certain internal geometries.

(iv) *Footprint*. importantly, these very large outer-scaled structures maintain a footprint in the near-wall region. This is clear from instantaneous DNS data (figure 7) and the wall-normal variation of $k_x\Phi_{uu}$ (figure 10). This input of low-wavenumber outer-scaled energy into the near-wall region supports the need for both inner and outer scaling (and hence Re_τ dependency) of the near-wall streamwise turbulence intensities.

(v) *Atmospheric surface layer*. we have anchored our observations with a single high Reynolds number measurement made in the atmosphere at $Re_\tau \approx 660000$. For periods of steady wind and neutral buoyancy, we confirm the presence and scaling of superstructures in high-Reynolds number turbulent boundary layers (§ 7).

(vi) *Possible origins*. numerous mechanisms have been suggested to explain the existence of large-scale features in the log and wake region of turbulent boundary layers, as discussed in § 1. At this stage the authors lack the time-resolved information required to comment on formation mechanisms. However, our recent experiences in the ASL, where scale separation between the near-wall structure and superstructure is more than three orders of magnitude different, makes us somewhat wary of 'wall-up'-type explanations. With increasing Reynolds number, the over-riding impression from our experiences at SLTEST and from the development of pronounced inner

and outer sites in the energy spectra (figure 10) is that the inner- and outer-scaled structure could in fact be two quite separate regimes that overlap and are intertwined in some complex Reynolds number-dependent manner.

The preceding analysis has dealt exclusively with streamwise velocity fluctuations. In future work we would like to expand the measurements made here to include the remaining two velocity components. Of particular interest are the pre-multiplied spectra for the spanwise fluctuations ($k_x \Phi_{vv}$), which are predicted to scale in a similar manner to the u spectra. This is also the component for which the least amount of experimental data presently exists.
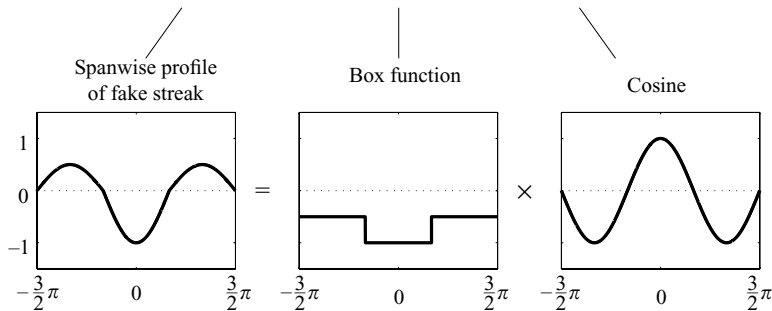
Appendix A. Functional form of synthetic flow fields

In §4.3, streamwise-aligned and spanwise-meandering synthetic streak arrays were considered (cases I and II respectively). The spanwise profile of case I is invariant in x, and given by

$$\text{case I:} \quad -\frac{3L_y}{2} < y_{fI} < \frac{3L_y}{2}, \quad 0 < x_{fI} < L_x$$

$$u_{fI}(y_{fI}, x_{fI}) = \left(-\frac{3}{4} - \frac{\cos(\pi y_{fI}/L_y)}{4\sqrt{\cos^2(\pi y_{fI}/L_y)}} \right) \cos\left(\frac{\pi y_{fI}}{L_y} \right), \quad (A\,1)$$

where L_y is the streak width and L_x is the streak length. The accompanying sketch shows that this function describes $1\frac{1}{2}$ periods of a co-sinusoid modulated by a box function such that the integral of the signal in the spanwise direction is zero. For the spanwise meandering features of case II, the original function (u_{fII}) has an x-dependent sinusoidal shift applied in the spanwise direction, of the form

$$u_{fII}\left(y_{fII}, x_{fII}\right) = u_{fI}, \quad (A\,2)$$

where

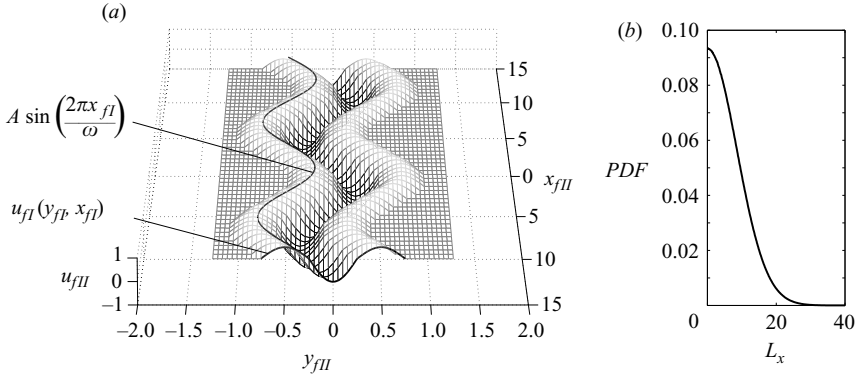$$y_{fII} = A \sin(2\pi x_f/\omega + \phi) + y_{fI}. \quad (A\,3)$$

FIGURE 15. (*a*) Case II: the meandering fake streak, as given by (A 2); (*b*) length scale distribution for L_x.

A and ω are the respective amplitude and period of the meander and ϕ (which is uniformly distributed between 0 and ω) randomizes the phase of the meander in x_f. A sketch of the meandering case is given in figure 15(*a*).

To create the full synthetic flow fields, the aligned or meandering features are randomly arranged with a normal distribution of length scales (about zero), yielding a mean length of $\overline{L}_x \approx 7\delta$ and a maximum length of approximately 30δ. Figure 15(*b*) shows the normalized probability distribution of L_x.

Appendix B. A note on energy spectra

The analysis of §4.3 shows that meandering may lead to misinference of length scales from one-dimensional energy spectra. In fact, there is potential for misinterpretation even when no meandering is present. Consider the pre-multiplied energy spectra for the streamwise-aligned case as shown by the solid line of figure 5(*d*). The peak in this curve occurs at 18δ, despite the fact that the average structural length for this case was just 6.9δ (as given by the distribution in figure 15*b*). Two important factors contribute to this discrepancy. In the first instance, the structure that we have modelled represents only approximately one half of a sinusoidal period in the streamwise direction. In such cases we would expect a spectral peak to occur at roughly twice the characteristic length scale. The actual streamwise profile used for the synthetic flows is a Hanning window of length L_x, which can be shown to yield a spectral peak at $1.717L_x$ (obtained by regression fit to a sinusoid). Thus it is clear that where flows are non-sinusoidally periodic (as turbulence indeed is) it is perhaps unwise to rely purely on a sinusoidal decomposition to infer structure. This factor alone does not fully account for the discrepancy in figure 5(*d*). There is an additional problem due to length scale distribution. Campbell's theorem tells us that randomly arranged events of equal length will return an energy spectrum identical in shape to that of a single isolated event. In this sense we might hope to be able to back-out structural information from energy spectra. However, in the presence of any form of distribution of length scales, Campbell's theorem informs us that the final energy spectrum will be a summation of the spectra for each individual length scale modulated by a density factor (probability × length scale). Thus the final spectral estimate (including the location of any pre-multiplied peak) is contaminated by the length scale distribution. The wide distribution of overlapping scales makes turbulent signals a prime candidate for this form of contamination.
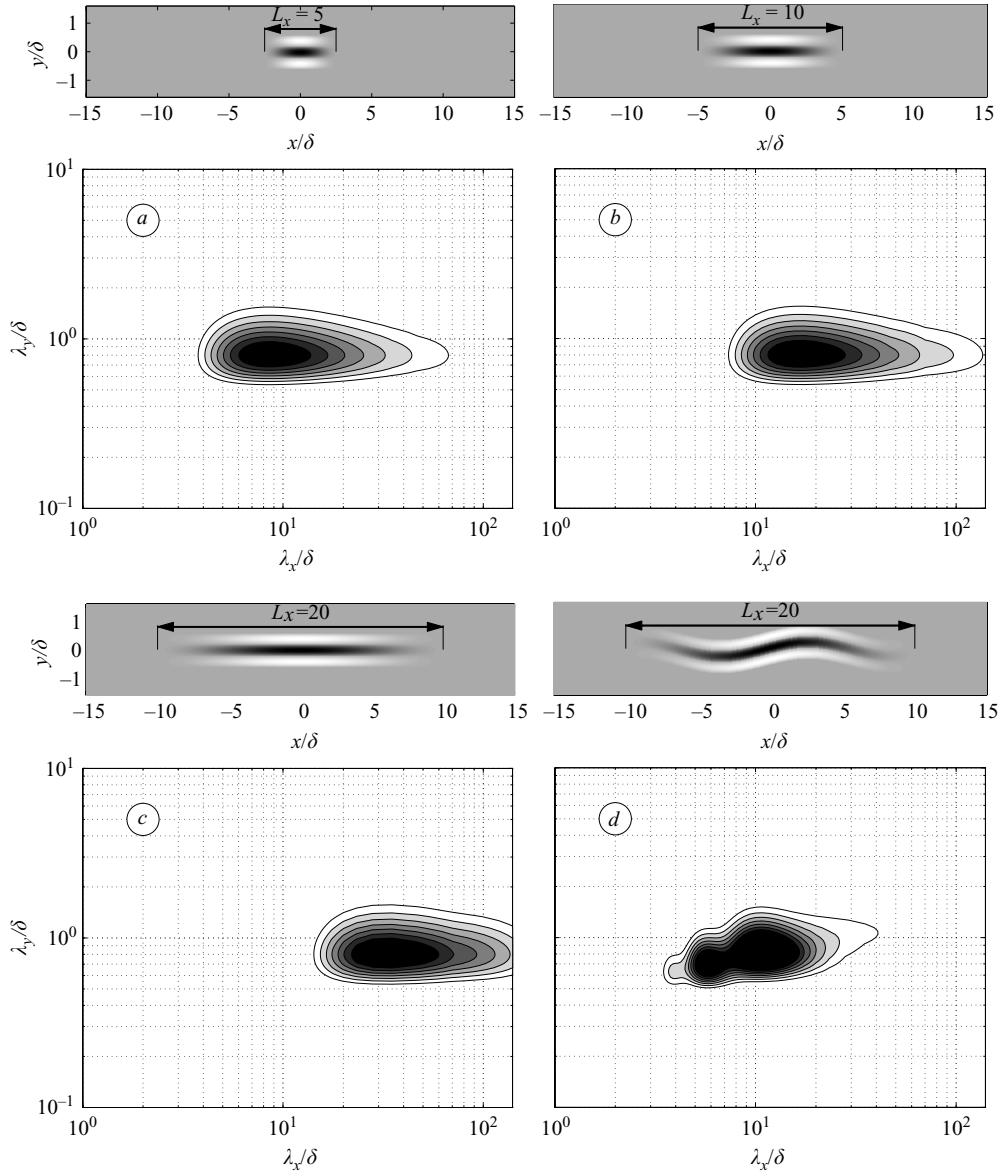
FIGURE 16. Two-dimensional premultiplied energy spectra for various isolated synthetic flow fields. Filled contours show normalized magnitude of $k_x k_y E_{uu}$ for (a) case I, streamwise-aligned $L_x = 5\delta$; (b) case I, streamwise-aligned $L = 10\delta$; (c) case I, streamwise-aligned $L = 20\delta$; (d) case II, meandering $L = 20\delta$. In each case a schematic of the synthetic flow is shown above the spectra (where the grey scale shows streamwise velocity fluctuation).

Two-dimensional spectra (E_{uu}) are not immune to these problems. Figure 16 shows $k_x k_y E_{uu}$ for various synthetic flow functions. Plots (a) to (c) show streamwise-aligned cases. For these single events, the peak in λ_x occurs at $1.717L_x$, as was previously predicted for the Hanning function. In the spanwise direction the peak in λ_y occurs at $2L_y$ (since the spanwise waveform is essentially sinusoidal). It is noted that in all cases the low wavenumber energy in the streamwise direction persists to approximately 10

times the peak value in λ_x. When analysing turbulent flow data it would be easy to misconstrue this tail in the low wavenumber energy as indicating the presence of very long structures. Yet for the synthetic flow fields under investigation there are no features with lengths greater than L_x. Figure 16(d) shows the $L_x = 20\delta$ case with meandering. The comparison between plots (c) and (d) highlights once again how the addition of meandering can shift the peak in the premultiplied spectra to shorter wavelengths. Not only this, but the meandering has also inclined the contours of $k_x k_y E_{uu}$ in the k_y direction. It is noted that contours of $k_x k_y E_{uu}$ calculated from DNS channel flows are tilted in this manner (del Álamo *et al.* 2004). It would be tempting to assume from the inclined contours of figure 16(d) that structures increase in width as they become longer. However, for the synthetic input structure used here, we know that this is not really the case. Rather, it is true that as structures become longer, they are statistically more likely to wander over a wider spanwise domain.

REFERENCES

ABE, H., KAWAMURA, H. & CHOI, H. 2004 Very large-scale structures and their effects on the wall shear-stress fluctuations in a turbulent channel flow up to $Re_\tau = 640$. *Trans. ASME: J. Fluids Engng* **126**, 835–843.

ADRIAN, R. J., MEINHART, C. D. & TOMKINS, C. D. 2000 Vortex organization in the outer region of the turbulent boundary layer. *J. Fluid Mech.* **422**, 1–54.

DEL ÁLAMO, J. C. & JIMÉNEZ, J. 2003 Spectra of the very large anisotropic scales in turbulent channels. *Phys. Fluids* **15**, 41–44.

DEL ÁLAMO, J. C., JIMÉNEZ, J., ZANDONADE, P. & MOSER, R. D. 2004 Scaling of the energy spectra of turbulent channels. *J. Fluid Mech.* **500**, 135–144.

BALINT, J.-L., WALLACE, J. M. & VUKOSLAVCEVIC, P. 1991 The velocity and vorticity vector fields of a turbulent boundary layer. Part 2. Statistical properties. *J. Fluid Mech.* **228**, 53–86.

BLACKWELDER, R. F. & KOVASZNAY, L. S. G. 1972 Time scales and correlations in a turbulent boundary layer. *Phys. Fluids* **15**, 1545–1554.

CHING, C., DJENIDI, L. & ANTONIA, R. 1995 Low-Reynolds-effects in a turbulent boundary layer. *Exps. Fluids* **19**, 61–68.

DEGRAAFF, D. B. & EATON, J. K. 2000 Reynolds number scaling of the flat-plate turbulent boundary layer. *J. Fluid Mech.* **422**, 319–346.

DROBINSKI, P., CARLOTTI, P., NEWSOM, R. K., BANTA, R. M., FOSTER, R. C. & REDELSPERGER, J.-L. 2004 The structure of the near-neutral atmospheric surface layer. *J. Atmos. Sci.* **61**, 699–714.

GANAPATHISUBRAMANI, B., HUTCHINS, N., HAMBLETON, W. T., LONGMIRE, E. K. & MARUSIC, I. 2005 Investigation of large-scale coherence in a turbulent boundary layer using two-point correlations. *J. Fluid Mech.* **524**, 57–80.

GANAPATHISUBRAMANI, B., LONGMIRE, E. K. & MARUSIC, I. 2003 Characteristics of vortex packets in turbulent boundary layers. *J. Fluid Mech.* **478**, 35–46.

GUALA, M., HOMMEMA, S. E. & ADRIAN, R. J. 2006 Large-scale and very-large-scale motions in turbulent pipe flow. *J. Fluid Mech.* **554**, 521–542.

HAFEZ, S., CHONG, M. S., MARUSIC, I. & JONES, M. B. 2004 Observations on high Reynolds number turbulent boundary layer measurements. In *Proc. 15th Australasian Fluid Mech. Conf* (ed. M. Behnia, W. Lin & G. D. McBain), Paper AFMC 00200. University of Sydney.

HAMBLETON, W. T., HUTCHINS, N. & MARUSIC, I. 2006 Multiple plane PIV measurements in a turbulent boundary layer. *J. Fluid Mech.* **560**, 53–64, in press.

HOYAS, S. & JIMÉNEZ, J. 2006 Scaling of the velocity fluctuations in turbulent channels up to $Re_\tau = 2003$. *Phys. Fluids* **18**, 011702.

HUNT, J. C. R. & MORRISON, J. F. 2000 Eddy structure in turbulent boundary layers. *Eur. J. Mech. B-Fluids* **19**, 673–694.

HUTCHINS, N., GANAPATHISUBRAMANI, B. & MARUSIC, I. 2004 Dominant spanwise Fourier modes, and the existence of very large scale coherence in turbulent boundary layers. In *Proc. 15th*

Australasian Fluid Mech. Conf. (ed. M. Behnia, W. Lin & G. D. McBain), Paper AFMC 00127. University of Sydney.

HUTCHINS, N., GANAPATHISUBRAMANI, B. & MARUSIC, I. 2005a Spanwise periodicity and the existence of very large scale coherence in turbulent boundary layers. In *Proc. Fourth Intl Symposium on Turbulence and Shear Flow Phenomena*, pp. 39–44. (TSFP4, Willamsburg, Virginia).

HUTCHINS, N., HAMBLETON, W. T. & MARUSIC, I. 2005b Inclined cross-stream stereo particle image velocimetry measurements in turbulent boundary layers. *J. Fluid Mech.* **541**, 21–54.

IWAMOTO, K., SUZUKI, Y. & KASAGI, N. 2002 Reynolds number effect on wall turbulence: Toward effective feedback control. *Intl J. Heat Fluid Flow* **23**, 678–689.

JIMÉNEZ, J. 1998 The largest scales of turbulent wall flows. In *CTR Annual Research Briefs*, pp. 943–945. Stanford University.

JIMÉNEZ, J. & DEL ÁLAMO, J. C. 2004 Computing turbulent channels at experimental Reynolds numbers. In *Proc. 15th Australasian Fluid Mech. Conf*. (ed. M. Behnia, W. Lin & G. D. McBain), Paper AFMC 00038. University of Sydney.

JIMÉNEZ, J., DEL ÁLAMO, J. C. & FLORES, O. 2004 The large-scale dynamics of near-wall turbulence. *J. Fluid Mech.* **505**, 179–199.

JIMÉNEZ, J. & PINELLI, A. 1999 The autonomous cycle of near-wall turbulence. *J. Fluid Mech.* **389**, 335–359.

JOHANSSON, A., HER, J.-Y. & HARITONIDIS, J. 1987 On the generation of high-amplitude wall-pressure peaks in turbulent boundary layers and spots. *J. Fluid Mech.* **175**, 119–142.

JOHANSSON, T. & KARLSSON, R. 1989 The energy budget in the near-wall region of a turbulent boundary layer. In *Applications of Laser Anemometry to Fluid Mechanics* (ed. R. Adrian, T. Asanuma, D. Durao, F. Durst & J. Whitelaw), pp. 3–22. Springer.

KIM, K. C. & ADRIAN, R. 1999 Very large-scale motion in the outer layer. *Phys. Fluids* **11**, 417–422.

KLEWICKI, J. C. & FALCO, R. E. 1990 On accurately measuring statistics associated with small scales in turbulent boundary layers using hot-wire probes. *J. Fluid Mech.* **219**, 119–142.

KLEWICKI, J. C., METZGER, M. M., KELNER, E. & THURLOW, E. M. 1995 Viscous sublayer flow visualizations at $R_\theta \cong 1500000$. *Phys. Fluids* **7**, 857–863.

KLINE, S. J., REYNOLDS, W. C., SCHRAUB, F. A. & RUNDSTADLER, P. W. 1967 The structure of turbulent boundary layers. *J. Fluid Mech.* **30**, 741–773.

KOVASZNAY, L. S. G. 1970 The turbulent boundary layer. *Annu. Rev. Fluid Mech.* **2**, 95–112.

KOVASZNAY, L. S. G., KIBENS, V. & BLACKWELDER, R. F. 1970 Large-scale motion in the intermittent region of a turbulent boundary layer. *J. Fluid Mech.* **41**, 283–326.

KUNKEL, G. J. & MARUSIC, I. 2006 Study of the near-wall-turbulent region of the high-Reynolds-number boundary layer using an atmospheric flow. *J. Fluid Mech.* **548**, 375–402.

LIGRANI, P. M. & BRADSHAW, P. 1987 Spatial resolution and measurement of turbulence in the viscous sublayer using subminiature hot-wire probes. *Exps. Fluids* **5**, 407–417.

MARUSIC, I. 2001 On the role of large-scale structures in wall turbulence. *Phys. Fluids* **13**, 735–743.

MARUSIC, I. & HUTCHINS, N. 2006 Experimental study of wall turbulence: Implications for control. In *Transition and Turbulence Control* (ed. M. Gad-el-Hak & H. M. Tsai). World Scientific.

MARUSIC, I. & KUNKEL, G. J. 2003 Streamwise turbulence intensity formulation for flat-plate boundary layers. *Phys. Fluids* **15**, 2461–2464.

MARUSIC, I. & PERRY, A. E. 1995 A wall wake model for the turbulent structure of boundary layers. Part 2. Further experimental support. *J. Fluid Mech.* **298**, 389–407.

MCLEAN, I. R. 1990 The near-wall eddy structure in an equilibrium turbulent boundary layer. PhD thesis, University of Southern California, USA.

METZGER, M. M. & KLEWICKI, J. C. 2001 A comparative study of near-wall turbulence in high and low Reynolds number boundary layers. *Phys. Fluids* **13**, pp. 692–701.

METZGER, M. M., KLEWICKI, J. C., BRADSHAW, K. L. & SADR, R. 2001 Scaling the near-wall axial turbulent stress in the zero pressure gradient boundary layer. *Phys. Fluids* **13**, 1819–1821.

MOSER, R. D., KIM, J. & MANSOUR, N. N. 1999 Direct numerical simulation of turbulent channel flow up to $Re_\tau = 590$. *Phys. Fluids* **11**, 943–945.

NAKAGAWA, H. & NEZU, I. 1981 Structure of space-time correlations of bursting phenomena in an open-channel flow. *J. Fluid Mech.* **104**, 1–43.

NICKELS, T. B., MARUSIC, I., HAFEZ, S. & CHONG, M. S. 2005 Evidence of the k_1^{-1} law in a high-Reynolds-number turbulent boundary layer. *Phys. Rev. Lett.* **95**, 074501.

PERRY, A. E., HENBEST, S. & CHONG, M. S. 1986 A theoretical and experimental study of wall turbulence. *J. Fluid Mech.* **165**, 163–199.

PERRY, A. E. & MARUSIC, I. 1995 A wall wake model for the turbulent structure of boundary layers. Part 1. Extension of the attached eddy hypothesis. *J. Fluid Mech.* **298**, 361–388.

PHILLIPS, W. R. C. 2003 Langmuir circulations. In *Wind over Waves II: Forecasting and Fundamentals of Applications* (ed. S. G. Sajjadi & J. C. R. Hunt), pp. 157–167. Horwood.

PURTELL, P., KLEBANOFF, P. & BUCKLEY, F. 1981 Turbulent boundary layer at low Reynolds number. *Phys. Fluids* **24**, 802–811.

RAO, K. N., NARASIMHA, R. & BADRI NARAYANAN, M. A. 1971 The 'bursting' phenomena in a turbulent boundary layer. *J. Fluid Mech.* **48**, 339–352.

SCHOPPA, W. & HUSSAIN, F. 2002 Coherent structure generation in near-wall turbulence. *J. Fluid Mech.* **453**, 57–108.

SPALART, P. R. 1988 Direct numerical simulation of a turbulent boundary layer upto $R_\theta = 1410$. *J. Fluid Mech.* **187**, 61–98.

TANAHASHI, M., KANG, S.-J., MIYAMOTO, T., SHIOKAWA, S. & MIYAUCHI, T. 2004 Scaling law of fine scale eddies in turbulent channel flows up to $Re_\tau = 800$. *Intl J. Heat Fluid Flow* **25**, 331–340.

TOH, S. & ITANO, T. 2005 Interaction between a large-scale structure and near-wall structures in channel flow. *J. Fluid Mech.* **524**, 249–262.

TOMKINS, C. D. & ADRIAN, R. J. 2003 Spanwise structure and scale growth in turbulent boundary layers. *J. Fluid Mech.* **490**, 37–74.

TOWNSEND, A. A. 1956 *The Structure of Turbulent Shear Flow*. Cambridge University Press.

TSUBOKURA, M. 2005 LES study on the large-scale motions of wall turbulence and their structural difference between plane channel and pipe flows. In *Proc. Fourth Intl Symposium on Turbulence and Shear Flow Phenomena*, pp. 1037–1042. TSFP4, Willamsburg, Virginia.

UEDA, H. & HINZE, J. O. 1975 Fine-structure turbulence in the wall region of a turbulent boundary layer. *J. Fluid Mech.* **67**, 125–143.

WARK, C. E., NAGUIB, A. M. & ROBINSON, S. K. 1991 Scaling of spanwise length scales in a turbulent boundary layer. *AIAA Paper* 91-0235.

WEI, T. & WILLMARTH, W. W. 1989 Reynolds-number effects on the structure of a turbulent channel flow. *J. Fluid Mech.* **204**, 57–95.

YOUNG, G. S., KRISTOVICH, D. A. R., HJELMFELT, M. R. & FOSTER, R. C. 2002 Rolls, streets, waves and more: A review of quasi-two-dimensional structures in the atmospheric boundary layer. *Bull: Am. Met. Soc.* **83**, 9971001.